Mechanisms and site requirements for NO and NH₃ oxidation on Cu/SSZ-13

Yilin Wang [a],[1], Runze Zhao [b],[1], Kenneth G. Rappé [a],[*], Yong Wang [a],[c], Fanglin Che [b],[*], Feng Gao [a],[*]

[a] *Institute for Integrated Catalysis, Pacific Northwest National Laboratory, Richland, WA 99354, USA*
[b] *Department of Chemical Engineering, University of Massachusetts Lowell, Lowell, MA 01854, USA*
[c] *The Gene and Linda Voiland School of Chemical Engineering and Bioengineering, Washington State University, Pullman, WA 99163, USA*

ARTICLE INFO

ABSTRACT

Two series of Cu/SSZ-13 catalysts were synthesized via aqueous solution and solid-state ion exchange using SSZ-13 supports of varying Si/Al ratios. The isolated and multinuclear Cu content of these catalysts were determined by H_2 temperature programmed reduction (H_2-TPR). Multinuclear Cu in these catalysts, including in situ Cu-dimers formed from $ZCu^{II}OH$ coupling and permanent CuO clusters, are active species for dry NO oxidation. NH_3 oxidation on these catalysts follows an internal SCR (i-SCR) mechanism, i.e., a portion of NH_3 is first oxidized to NO, then NO is selectively reduced by the remaining NH_3 to N_2. NH_3 oxidation displays distinct kinetic behavior below ~300 °C and above ~400 °C. At low temperature the results indicate that NH_3-solvated mobile Cu-ions are the active centers. CuO clusters, when present, also contribute to the low temperature activity by catalyzing NH_3 oxidation to NO. At high temperature, in situ Cu-dimers and CuO clusters catalyze NH_3 oxidation to NO, and isolated Cu-ions catalyze SCR to realize the cascade turnovers. For both NO and NH_3 oxidation, Cu-dimers balanced by framework charges of close proximity appear to be more active than Cu-dimers balanced by distant framework charges. However, the former Cu-dimers are less stable than the latter and tend to split into monomers in the presence of vicinal Brønsted acid sites. Via density functional theory (DFT) calculations, the i-SCR mechanism for low temperature NH_3 oxidation, i.e., the energetic favorability for the involvement of the NO intermediate, is justified. The DFT results also agree with experimental data that the formation of Cu-dimers from $ZCu^{II}OH$ dimerization is essential for NH_3 oxidation at high temperature.

1. Introduction

In energy generation processes via lean fuel combustion, NOx (NO and NO_2) are unavoidable side products. Their elimination is typically achieved by ammonia selective catalytic reduction (NH_3-SCR) reactions, in particular standard SCR ($4NO + 4NH_3 + O_2 = 4\,N_2 + 6\,H_2O$) and fast SCR ($NO + NO_2 + 2NH_3 = 2\,N_2 + 3\,H_2O$) [1–3]. In such processes, ammonia typically originates from urea hydrolysis. To achieve high NOx elimination efficiency, excess urea is often applied leading to "ammonia slip" that causes negative environmental impacts, the same as urea fertilizer volatilization that plagues the agriculture sector [4]. Fortunately, ammonia slip can be readily eliminated by the so-called selective catalytic oxidation (NH_3-SCO) process, i.e., $4NH_3 + 3\,O_2 = 2\,N_2 + 6\,H_2O$, over an ammonia slip catalyst (ASC) employed downstream of SCR [5,6].

NH_3-SCO can be catalyzed by a wide variety of catalysts including noble metals, transition metal oxides, and metal-exchanged zeolites. Cu-

and/or Fe-exchanged zeolites have received much attention due to their low cost, environmentally friendly nature, high activity and N_2 selectivity [7,8]. Two prevailing NH_3-SCO mechanisms have been reported in literature:

1. The hydrazine mechanism, i.e., NH_3 is activated to $-NH_2$, and $-NH_2$ couples to a hydrazine (NH_2-NH_2) intermediate that then is oxidized to N_2 and H_2O, and
2. The internal SCR (i-SCR) mechanism, i.e., a portion of NH_3 is first oxidized to NO, and N_2 formation follows the SCR mechanism between NO and remaining NH_3 [7,8].

In studying SCO over Fe-exchanged zeolites, Yang and coworkers discovered that catalysts displaying higher SCR activity also showed higher N_2 selectivity in SCO. This led the authors to conclude that NH_3-SCO follows the i-SCR mechanism [9]. Similar to Fe-exchanged zeolites, Cu-exchanged zeolites are typically excellent SCR catalysts. As such, the

same i-SCR mechanism is also anticipated, provided that NH_3 oxidation to NO is enabled over Cu-zeolites. Indeed, by introducing small contents of noble metals or CuO particles to Cu-zeolites to boost NH_3 oxidation to NO, low-temperature NH_3-SCO activity can be improved without sacrificing N_2 selectivity [10,11]. For the same reason, some state-of-the-art NH_3-SCO catalysts adopt layered structures containing both supported noble metal and metal-exchanged zeolite phases [5–8].

Cu/SSZ-13 (or Cu/CHA) is the current state-of-the-art commercial NH_3-SCR catalyst for diesel engine exhaust abatement. Unsurprisingly, SCR mechanistic research over Cu/CHA has been intensive in recent years [12–22]. In many SCR studies, NH_3 oxidation has been included since it is an important side reaction of SCR [12, 13, 23–44]. Unfortunately, clear mechanistic insights into NH_3 oxidation over Cu/CHA have hardly been made. In the present study, we prepared two series of Cu/CHA catalysts with systematic variations on Cu speciation, and then carried out NH_3 oxidation to elucidate mechanism and site requirement. We also studied NO oxidation as a probe reaction; on Cu/CHA, this latter reaction is known to occur on multinuclear Cu sites but not on isolated Cu-ions [45]. To gain further molecular insights into the mechanism and site requirements, we then performed density functional theory (DFT) calculations on the energy diagrams of the i-SCR pathways on NH_3-solvated Cu-ions at the low temperature regime. Our DFT study also focused on how isolated Cu-ions (e.g., $ZCu^{II}OH$) transform into multinuclear Cu moieties (e.g., Cu-O-Cu dimers), and how such sites activate NH_3 at high temperature. This study aims to provide fundamental understandings of NH_3 oxidation mechanisms on Cu/CHA. Moreover, since multinuclear Cu moieties in zeolites have recently been demonstrated to activate methane [46–48], we hope this study also useful for researcher in that research area and beyond.

2. Methods

2.1. Experimental

2.1.1. Catalyst synthesis

Na/CHA zeolite supports with SiAl = 6, 12, 18, 24, 30 and 36 were hydrothermally synthesized in house using TMAda-OH (Sachem Inc., 25% N,N,N-trimethyl-1-adamantyl ammonium hydroxide) as the structure-directing agent (SDA), $Al(OH)_3$ (Sigma Aldrich, ~54% Al_2O_3) as the Al source, LUDOX AS-30 colloidal silica (Sigma Aldrich, 30 wt% suspension in H_2O) as the Si source, and NaOH (Sigma Aldrich, 99.9%) and deionized water. Gel compositions were 1TMAda-OH: 1NaOH: xAl_2O_3: $10SiO_2$: 220 H_2O, where "x" varies to enable different Si/Al ratios. The gel ingredients were mixed under stirring according to a specific sequence detailed elsewhere [49]. Upon homogenization, the gel was sealed in a 125-ml Teflon-lined stainless-steel autoclave containing a magnetic stir bar. The autoclave was placed in a sand batch on top of a hot plate stirrer. Hydrothermal synthesis was carried out at 160 °C under continuous stirring at 400 rpm for 4 days. After synthesis, the solid zeolite was separated from the suspension by centrifugation and washed three times with deionized water. It was then dried under an air flow at 60 °C overnight and calcined in static air at 650 °C for 5 h to burn off the SDA. NH_4/CHA was obtained by ion exchange of the as-prepared Na/CHA zeolite with excess 0.1 M NH_4NO_3 solution at 80 °C for 2 h. The process was repeated one time to ensure complete Na^+ removal.

The first series of Cu/CHA catalysts were prepared by aqueous solution ion exchange (AIE), where the NH_4/CHA supports were exchanged with 0.01 M $Cu(NO_3)_2$ (Sigma Aldrich, 99.99%) solution (1 g of solid per 100 ml of solution) at 80 °C for 2 h under stirring. To avoid the formation of CuO clusters, the pH of the suspension was kept at ~2.0 with 0.1 M HNO_3 (Sigma Aldrich, analytical grade). The exchange process was repeated three times to generate Cu/CHA with "saturated" Cu loadings. Following ion exchange, the solid was recovered by centrifugation, dried in air, and then calcined in static air at 650 °C for 5 h. These AIE catalysts are denoted Cu-X where "X" represents Si/Al ratio

of the corresponding SSZ-13 support. The second series of Cu/CHA catalysts were prepared by solid-state ion exchange (SSIE). NH_4/CHA supports were first calcined in air at 550 °C for 2 h to convert into H-form. $Cu(NO_3)_2$ was loaded on the H-form supports via incipient wetness impregnation. For every gram of zeolite solid, 0.6 ml of deionized H_2O was used to dissolve 0.055 g of $Cu(NO_3)_2·2.5 H_2O$ for the impregnation, leading to a nominal Cu loading for this series of samples ~1.5 wt%. After drying in air, the samples were calcined in static air at 800 °C for 5 h. Note that $Cu(NO_3)_2$ decomposes to CuO at rather low temperatures; the nature of this synthesis is solid-state ion exchange between zeolitic protons and CuO [33,50]. These SSIE catalysts are denoted Cu-Xs, where "X" again represents Si/Al ratio of the corresponding support.

2.1.2. Catalyst characterization

Cu contents of all AIE and selected SSIE catalysts were determined with Inductively Coupled Plasma Atomic Emission Spectroscopy (ICP-AES) at Galbraith Laboratories (Knoxville, TN, USA).

Specific surface area (BET method) and micropore volume (t-plot method) of the catalysts were measured with a Quantachrome Autosorb-6 analyzer with liquid N_2 adsorption. The catalysts were degassed under high vacuum overnight at 250 °C prior to analysis. Powder X-ray diffraction (XRD) measurements were performed on a Philips PW3040/ 00 X′ Pert powder X-ray diffractometer with Cu Kα radiation (λ = 1.5406 Å). Data were collected with 2θ ranging from 5° to 50° using a step size of 0.01°.

Temperature-programmed reduction with H_2 (H_2-TPR) measurements were carried out on a Micromeritics AutoChem 2920 apparatus. A mass of ~100 mg catalyst was used for each experiment. The catalyst was first purged with N_2, and then switched to ~10% H_2/Ar (50 ml/min) at room temperature until the thermal conductivity detector (TCD) signals stabilized. Thereafter, the sample was ramped from ambient to 1200 °C at a rate of 10 °C/min and maintained at 1200 °C until no H_2 consumption was measured. To quantify H_2 consumption, CuO (Sigma Aldrich, 99.9%) reduction with the same procedure was used as the standard.

2.1.3. Reaction tests

NH_3 oxidation "light-off" tests were conducted on a custom-built plug-flow reaction test stand equipped with an online MKS MultiGas 2030 FTIR gas analyzer with the gas cell retained at 191 °C for measuring concentrations of the reactants and products. A mass of 120 mg of sieved catalyst (40–60 mesh) was supported on a quartz frit inside a 0.8-cm inner diameter quartz reactor placed in an electric tube furnace. The composition of the gas feed was 380 ppm NH_3, 10% O_2, 2.5% H_2O, and balanced N_2. The total flow rate was 600 ml/min, and the gas hourly space velocity (GHSV) was estimated to be 200,000 h^{-1}. Activity measurements were conducted from 550 to 100 °C at temperatures decreasing stepwise at intervals of 50 or 20 °C. Reaction at each temperature was maintained for at least 45 min to reach steady state.

NO oxidation tests ($2NO + O_2 = 2NO_2$) were carried out in a similar manner. The composition of the gas feed was 380 ppm NO (contains ~10 ppm NO_2 impurity), 10% O_2, and balance N_2. Note that H_2O was not added to the reaction feed; this is because NO oxidation in this context is to serve as a probe reaction which is known to occur on multinuclear Cu sites but not on isolated Cu-ions [45]. NO and NH_3 conversions were calculated using the following equations:

$$NO \quad conversion = \frac{(NO)_{inlet} - (NO)_{outlet}}{(NO)_{inlet}} \times 100\% \tag{1}$$

$$NH_3 \quad conversion = \frac{(NH_3)_{inlet} - (NH_3)_{outlet}}{(NH_3)_{inlet}} \times 100\% \tag{2}$$

2.2. Computational

DFT calculations were performed using the Vienna Ab-initio Simu-

lation Package (VASP) software package [51]. The Perdew-Burke-Ernzerhof (PBE) functional was used for all calculations [52,53]. The electron-ion interactions were described using projected augmented wave (PAW) potentials. Geometries were optimized when the maximum force and energy difference between each self-consistency loop on each atom were less than 0.03 eV/Å and 10^{-4} eV, respectively. The plane-wave basis set with an energy cutoff of 400 eV was used for the electronic structure calculations. The Brillouin zone was sampled using a Monkhorst-Pack k-point mesh of $3 \times 3 \times 3$ [54].

Adsorption energies (E_{ads}) of reaction intermediates and reaction energies (ΔH_{rxn}) of NH_3-activation related reactions were calculated by the following equations:

$$E_{ads} = E_{total} - E_{Cu/SSZ-13} - E_{adsorbate} \tag{3}$$

$$\Delta H_{rxn} = E_{FS} - E_{IS} \tag{4}$$

where E_{total} denotes the total energy of our Cu/CHA model structure with adsorbed species, $E_{Cu/SSZ-13}$ is the energy of the Cu/CHA model structure alone, and $E_{adsorbate}$ is the isolated adsorbate (molecule/radical) in the gas phase. The reaction energy ΔH_{rxn} is calculated as the energy difference between the final state (E_{FS}) and initial state (E_{IS}) of the reaction of interest.

Bader charge analysis was carried out to study the dynamic nature of the Cu oxidation states during NH_3 oxidation [55,56]. Based on our benchmarking Bader charge analysis, Cu in Z_2Cu^{II} has a Bader charge of ~1e, while that in ZCu^I has a Bader charge of ~0.5e; these values are consistent with the previous theoretical reports [56–58]. To study isolated Cu-ion configurations and possible dimerization of such isolated ions to dimers, we utilized two chabazite unit cell structures with a Si/Al ratio of 11 (Fig. S1):

1. The rhombohedral unit cell with a = 9.36 Å, b = 9.48 Å, and c = 9.36 Å, comprising 12 T atoms (11 Si, 1 Al) and 24 O atoms [52], and
2. The dual-rhombohedral unit cell with a = 18.72 Å, b = 9.48 Å, and c = 9.36 Å, comprising 24 T atoms (22 Si, 2 Al) and 48 O atoms.

A Si/Al ratio of 11 was chosen to closely represent current state-of-the-art CHA catalysts and to aid in the simplification of CHA topology arrangement for DFT calculations. Additional computational details can be found in the SI.

3. Results and Discussion

Specific surface areas (including micropore and external surfaces) and micropore volumes of the Na-form zeolite supports and the two series of Cu-exchanged catalysts are tabulated in Table S1 of the Supporting Information (SI). Powder XRD patterns of the two series of catalysts are presented in Fig. S2a-d. These catalyst materials display textural properties typical for highly crystalline chabazite, and additional detailed descriptions of these results are included in the SI.

3.1. Cu speciation studied by H_2-TPR

To gain details on Cu speciation, H_2-TPR was carried out on ambient hydrated catalysts, and the results are shown in Figs. 1a and 1b for the AIE and SSIE samples, respectively. For interpreting these results, it is important to first summarize key prior findings regarding Cu quantification via H_2-TPR of (1) isolated Cu^{II}-ions and (2) other Cu moieties. Regarding (1), the two types of isolated Cu^{II}-ions in Cu/CHA (i.e., Z_2Cu^{II} balanced by two framework negative charges and $ZCu^{II}OH$ balanced by one framework negative charge; Z = AlO_4) follow a sequential reduction, i.e., $Cu^{II} \rightarrow Cu^I \rightarrow Cu^0$ [3,28,59,60]. More specifically, $ZCu^{II}OH$ reduces to ZCu^I slightly above 200 °C, whereas Z_2Cu^{II} reduces to ZCu^I around 300–500 °C [12, 49, 61–66]. ZCu^I formed from Z_2Cu^{II} or $ZCu^{II}OH$ is subsequently indistinguishable and reduces to Cu^0 at very
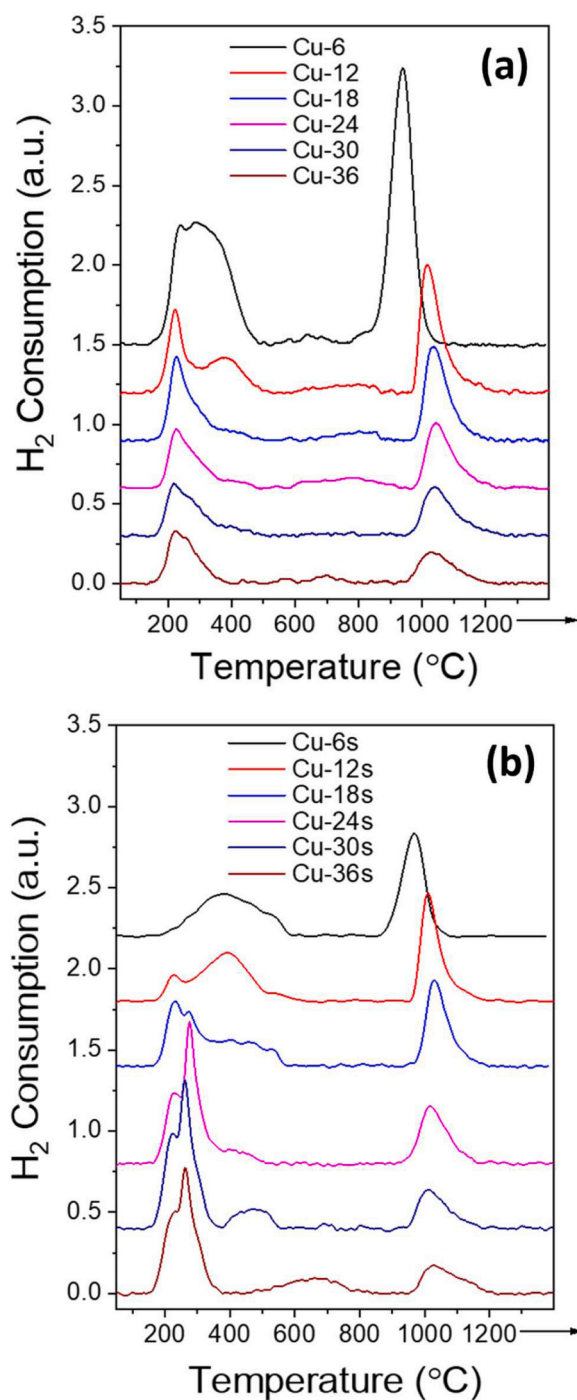

Fig. 1. Hydrogen temperature programmed reduction (H_2-TPR) profiles for (**a**) the AIE catalysts, and (**b**) the SSIE catalysts.

high temperatures, typically above 800 °C [12,49,67]. Regarding (2), other Cu moieties such as CuO clusters, Cu-aluminates and Cu-sulfates, typically found in catalysts that contain excess Cu (or in catalysts that have experienced dealumination, e.g., with hydrothermal treatment, or sulfur contamination), reduce directly to Cu^0, i.e., $Cu^{II} \rightarrow Cu^0$ [67–69]. More specifically, CuO clusters reduce around 300 °C; reduction temperatures for Cu-aluminates and Cu-sulfates can vary rather substantially but are typically well below ZCu^I reduction temperatures (>800 °C) [33,49,70].

As shown in Fig. 1a, the AIE samples display strong H_2 consumption below ~500 °C and above ~900 °C; weak H_2 consumption is also found between these two temperatures. Based on the prior discoveries

described above, two assumptions are made here for our Cu quantification: (1) ZCu^I is exclusively reduced to Cu^0 above 800 °C; this serves as our basis for the quantification of isolated Cu-ions; (2) multinuclear Cu moieties (CuO clusters and, less likely, Cu-aluminates) are reduced to Cu^0 below 800 °C; as such, the difference in H_2 consumption below and above 800 °C is indicative of multinuclear Cu moieties. Detailed peak area analysis and the calculated isolated Cu-ion percentages of the AIE samples are tabulated in Table S2. These results demonstrate the dominance of isolated Cu-ions in these samples. Total Cu contents measured via ICP-AES is shown in Table 1; based on these results and the H_2-TPR analysis, isolated Cu-ion contents of the AIE samples are readily calculated and the results are also presented in Table 1. Since the $Cu^{II} \rightarrow Cu^I$ reduction for $ZCu^{II}OH$ occurs at lower temperatures than that of Z_2Cu^{II} [12, 49, 61–66], it is further possible to conduct Z_2Cu^{II} and $ZCu^{II}OH$ quantification by peak fitting of the low-temperature TPR profiles. Fig. S3 presents a peak fitting example on low temperature H_2 consumption of the Cu-12 sample with the Gaussian function. We note that it is nearly impossible to reliably isolate the small contents of CuO within this series of samples by peak fitting. As such, its presence is ignored here; this treatment inevitably introduces small errors to Z_2Cu^{II} and $ZCu^{II}OH$ quantification. Based on peak fitting, Z_2Cu^{II} and $ZCu^{II}OH$, contents of the AIE samples are estimated. Combined with the multinuclear Cu estimate from above, the wt% results of Z_2Cu^{II}, $ZCu^{II}OH$, and CuO are presented in Table S3a; Table S3b presents these contents normalized to the total Cu content of the samples. It is readily seen from Table S3a and Table S3b that Cu-6 contains more Z_2Cu^{II} than $ZCu^{II}OH$, Cu-12 contains comparable amounts of both species, and the remaining samples with higher Si/Al ratios contain mostly $ZCu^{II}OH$. Such a speciation trend is consistent with the computed Cu site compositional phase diagram as a function of Si/Al and Cu/Al ratios [15].

H_2-TPR results for the SSIE samples are shown in Fig. 1b. In the low temperature regime, all samples except Cu-6 s display a reduction state at ~230 °C that is readily attributed to $ZCu^{II}OH$. Samples with Si/Al $\geq$ 18 also display a sharp reduction state at ~300 °C that can be safely assigned to CuO clusters [33,67]. Samples with Si/Al $\leq$ 18 also display a broad reduction peak centered at ~400 °C due to Z_2Cu^{II}. Since SSIE was carried out at 800 °C where high-temperature stable phases like Cu-aluminates can form between CuO and extraframework Al, weak H_2 consumption at ~550 °C for some of the samples (~700 °C for Cu-36 s) is likely due to reduction of such minor moieties. In the high temperature regime (> 800 °C), all samples display sharp ZCu^I reduction. Again, by assuming that ZCu^I only reduces above 800 °C, isolated Cu percentages are readily calculated by the same peak area analysis described above, and the results are shown in Table S4. Expectedly, isolated Cu percentage decreases monotonically with increasing Si/Al ratio of the support. Total Cu contents of the SSIE samples (isolated and multinuclear) was confirmed at ~1.50 wt% through ICP-AES analysis on select samples. This is expected and known from the SSIE synthesis procedure, which contrasts with the AIE procedure where Cu uptake is not known and thus ICP-AES is necessary to determine total Cu content. Thus, isolated Cu contents for the SSIE series of samples are calculated based on the H_2-TPR results using ~1.50 wt% total Cu loading, and the results are tabulated in Table 2. We also attempted peak fitting to obtain Z_2Cu^{II} and $ZCu^{II}OH$ contents of this series of samples. However, the intimate overlapping between isolated Cu-ions and CuO clusters makes reliable

Table 1
Total and isolated Cu content of the AIE catalysts[**].

Sample	Cu-6	Cu-12	Cu-18	Cu-24	Cu-30	Cu-36
Total Cu content (wt%)	3.69	1.72	1.48	1.17	1.05	0.98
Isolated Cu content (wt%)	3.59	1.66	1.41	1.01	0.97	0.74
Cu-ion/Al ratio	0.24	0.20	0.25	0.24	0.28	0.26

[**] Total Cu content measured via ICP-AES; isolated Cu content derived from H_2-TPR

Table 2
Total and isolated Cu content of the SSIE catalysts[**].

Sample	Cu-6 s	Cu-12 s	Cu-18 s	Cu-24 s	Cu-30 s	Cu-36 s
Total Cu content (wt%)	1.50	1.50	1.50	1.50	1.50	1.50
Isolated Cu content (wt%)	1.41	1.34	1.16	0.96	0.68	0.61
Cu-ion/Al ratio	0.09	0.16	0.21	0.23	0.20	0.21

[**] Total Cu content determined from SSIE synthesis; isolated Cu content derived from H_2-TPR

quantification challenging. During peak fitting, we therefore gave highest priority to the accuracy of the 230 °C reduction peak (due to $ZCu^{II}OH$). Upon determination of the $ZCu^{II}OH$ contents, we then back calculated Z_2Cu^{II} contents based on total isolated Cu-ion contents of these samples. These results combined with the estimate of multinuclear Cu content are tabulated in Table S5a for the SSIE samples, and Table S5b presents these wt% contents normalized to the total Cu content of the samples.

To further verify quality of our Cu quantification data shown in Table 1 and Table 2, we also examined the consistency between H_2-TPR and ICP (Fig. S4), and cross-checked isolated Cu quantification between the two series of samples (Fig. S5). In short, good accuracy is readily achieved by utilizing high-temperature ZCu^I reduction peaks for the quantification of total isolated Cu contents (Tables 1 and 2). However, further quantification of Z_2Cu^{II} and $ZCu^{II}OH$ contents (Table S3a-b, S5a-b) based on peak fitting of the (sometimes heavily overlapped) low temperature reduction states, should be considered less accurate. In any case, the isolated Cu-ion quantification results collectively demonstrate that low Si/Al ratio favors Z_2Cu^{II} population and high Si/Al ratio favors $ZCu^{II}OH$ population despite of the synthesis method. As such, the formation of $ZCu^{II}OH$ and Z_2Cu^{II} during SSIE can be described by reactions R1 and R2 below, where [CuO] denotes a "molecular" CuO unit.

$$ZH + [CuO] \rightarrow ZCu^{II}OH \tag{R1}$$

$$ZH + ZCu^{II}OH \rightarrow Z_2Cu^{II} + H_2O \tag{R2}$$

R1 can be considered to occur at 8-membered ring openings of the CHA support surface that contain at least one framework Al, allowing $[Cu^{II}OH]^+$ to form and then diffuse into the CHA cage. When paired Al sites (-Al-Si-Al- or -Al-Si-Si-Al-) are available, as in the case of low Si/Al ratios, $ZCu^{II}OH$ further converts to Z_2Cu^{II} via R2. This chemistry is driven by the fact that Z_2Cu^{II} is thermodynamically more stable than $ZCu^{II}OH$ [71,72]. When paired Al site contents are limited, as in the case of high Si/Al ratios, the probability of R2 is low. It is very important to note, however, that $ZCu^{II}OH$ can populate prior to Z_2Cu^{II} saturation due to kinetic stabilization [73], and Z_2Cu^{II} can readily hydrolyze to $ZCu^{II}OH$ under low temperature SCR conditions [21].

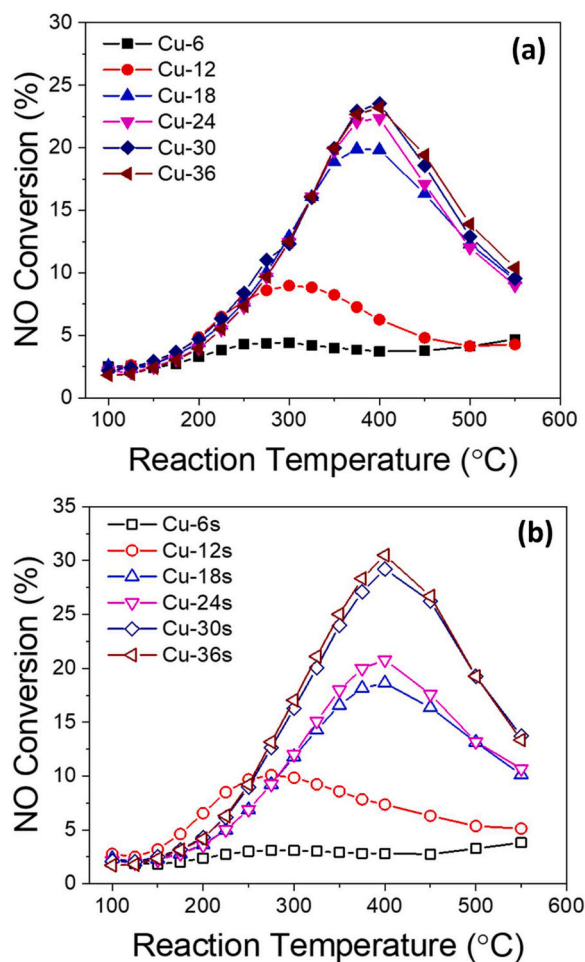*3.2. NO oxidation*

Fig. 2a and Fig. 2b depict NO conversion vs. temperature plots for "dry" NO oxidation ($2NO + O_2 \rightarrow 2NO_2$) over the AIE and SSIE catalysts, respectively. For the AIE catalysts, samples with Si/Al $\geq$ 18 display similar NO conversions at all temperatures. Over these catalysts, NO conversions reach their highest values at ~400 °C, and then decrease monotonically with increasing temperature. This is because these catalysts become active in catalyzing the reverse reaction ($2NO_2 \rightarrow 2NO + O_2$) at such high temperatures [74]. Below ~250 °C, the Cu-12 sample maintains similar NO conversions to the higher Si/Al samples; however, NO conversions decline above ~300 °C. The Cu-6 sample displays similar kinetic behavior to Cu-12, yet with even lower NO conversions. Two points are worth noting regarding the distinct kinetic behavior of Cu-6 and Cu-12 as compared to other samples:
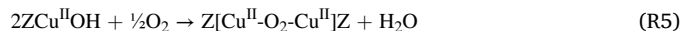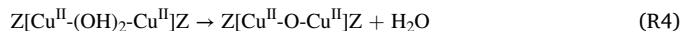
Fig. 2. NO conversion vs. temperature plots in steady state dry NO oxidation over (**a**) AIE, and (**b**) SSIE catalysts. 120 mg catalyst was used; reactant composition included 380 ppm NO (contains ~10 ppm NO_2 impurity), 10% O_2, and balanced N_2; the total flow rate was 600 ml/min, and the gas hourly space velocity (GHSV) was estimated to be 200,000 h^{-1}.

1. NO conversion decline with increasing temperature over Cu-6 and Cu-12 must be due to reasons other than reverse NO oxidation, and
2. Not all Cu species are equally active for NO oxidation; note particularly that Cu-6 has the highest Cu loading but achieves the lowest NO conversion.

As shown in Fig. 2**b**, the SSIE samples display similar Si/Al ratio-dependent kinetic behavior to the AIE catalysts for NO oxidation. Particularly, the 4 higher Si/Al catalysts show NO conversion decline at ~400 °C, while that over Cu-6 s and Cu-12 s occurs at lower temperatures. The SSIE samples also display unique kinetic behavior that unlike the AIE samples. Note that while Cu-6 s displays the lowest NO conversions, Cu-12 s shows highest NO conversions below ~250 °C. Furthermore, Cu-18 s and Cu-24 s show highly similar NO conversions at all temperatures, and the same is true for Cu-30 s and Cu-36 s
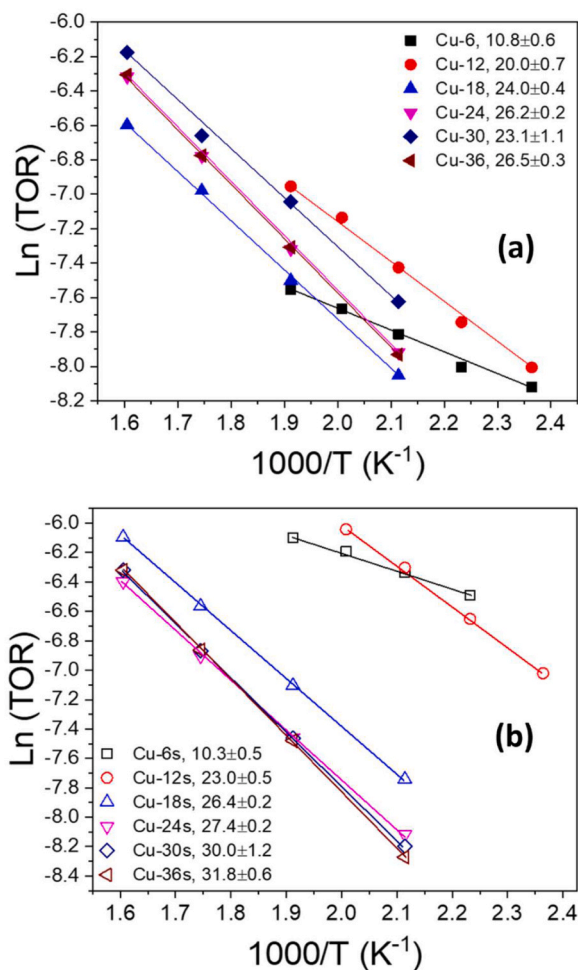
Prior to additional quantitative description of the data shown in Figs. 2**a** and 2**b**, it is useful to summarize relevant literature studies on NO oxidation over Cu/CHA. According to Verma et al. [45], dry NO oxidation on Cu/CHA only occurs on multinuclear Cu_xO_y species but not isolated Cu-ions. Over a series of Cu/CHA catalysts with Si/Al ~ 4.5, they found no catalytic activity for samples with Cu/Al < 0.2, and for samples with higher Cu/Al ratios, they found that NO conversion rates correlated linearly with Cu_xO_y contents quantified by in situ XANES. The authors further suggested on the basis of DFT calculations that key Cu_xO_y species are Cu-dimers (e.g., Z[Cu_2O]Z and Z[Cu_2O_2]Z), and

dimers balanced by framework Al with different proximity possess different activity. More recently, a few groups used in situ UV–vis spectroscopy, among other techniques, to further probe the nature and formation mechanisms of multinuclear Cu in Cu/CHA [75–78]. The most important consensus of such studies is the formation of dimers from $ZCu^{II}OH$ of suitable proximity. The following simplified reaction pathways can be used to describe Cu-dimer formation.

$$2ZCu^{II}OH \rightarrow Z[Cu^{II}-(OH)_2-Cu^{II}]Z \qquad (R3)$$

$$Z[Cu^{II}-(OH)_2-Cu^{II}]Z \rightarrow Z[Cu^{II}-O-Cu^{II}]Z + H_2O \qquad (R4)$$

$$2ZCu^{II}OH + \tfrac{1}{2}O_2 \rightarrow Z[Cu^{II}-O_2-Cu^{II}]Z + H_2O \qquad (R5)$$

Furthermore, Li et al. [77] discovered that, in CHA containing only isolated Al T-sites, $ZCu^{II}OH$ is always accompanied with O- or OH-bridged Cu dimers and/or larger aggregates even at intermediate Cu/Al ratios. In a recent UV–vis spectroscopy and DFT study, Zhang et al. [78] demonstrated both $ZCu^{II}OH$ dimerization in O_2, and reactivity of the Cu-dimers toward NO oxidation. In contrast, Z_2Cu^{II} does not dimerize in the presence of O_2, and is thus inactive for NO oxidation.

Based on these prior studies, the NO conversion data in Figs. 2**a** and 2**b** were normalized to turnover rates (TORs, mole NO $mole_{Cu}^{-1}$ s^{-1}) with respect to the non-Z_2Cu^{II} contents of the catalysts (Table S3, S5), and the low temperature portion were further subjected to Arrhenius analysis. The Arrhenius plots are shown in Fig. 3, where apparent activation energy (Ea) values are marked next to the corresponding sample labels.

Fig. 3. Arrhenius plots derived using low-temperature NOx conversion data shown in Fig. 2. (**a**) AIE samples, (**b**) SSIE samples. Apparent reaction activation energies are marked next to the corresponding sample labels.

It is important to note that the lack of detailed in situ Cu speciation information, i.e., percentages of $ZCu^{II}OH$ that dimerize and become catalytically active during NO oxidation, and sizes and dispersions of larger CuO clusters, the TOR values should be considered semi-quantitative, and their comparisons may not lead to rigorous conclusions. However, since Ea calculations are not affected by such uncertainties, it is our belief that certain rigorous conclusions can still be derived by comparing the Ea values.

Both series of catalysts display Ea values that are dependent on the support Si/Al ratio. For the AIE samples, Cu-6 displays the lowest Ea value = ~11 kJ/mol, Cu-12 displays the second lowest Ea value = ~20 kJ/mol, and the other 4 catalysts present Ea values = ~23–27 kJ/mol that show no consistent trend with Si/Al ratio. For the SSIE samples, Cu-6 s displays the lowest Ea value = ~10 kJ/mol, and the other samples display Ea values = ~23 to ~31 kJ/mol that consistently increase with increasing Si/Al. Together with the Cu speciation data shown in Table S2–S5, we propose the following:

1. Cu dimers balanced by framework Al at close proximity (e.g., within the same 6- or 8-membered rings, common for low Si/Al ratios) offer more facile NO oxidation pathways than Cu-dimers balanced by framework Al farther apart (e.g., within different rings of the chabazite cage, common for high Si/Al ratios). Note that prior DFT calculations already suggested such activity difference [45].
2. Cu-dimers balanced by distant framework Al display NO oxidation properties similar to those of larger CuO clusters.
3. $ZCu^{II}OH$ dimerization efficiency is dependent on both support Si/Al ratio and temperature. For catalysts with high densities of residual Brønsted acid sites (i.e., SiAl = 6 or 12), Cu-dimers tend to split back to isolated Cu-ions at < 300 °C, causing NO conversion to decrease. This latter phenomenon is rooted in the temperature-dependent relative stability between Z_2Cu^{II} and $ZCu^{II}OH$ that has been discussed earlier, i.e., $ZCu^{II}OH$ prefers to convert to Z_2Cu^{II} (R2) rather than to dimers (R3-R5) above ~300 °C on condition that Brønsted acid sites of suitable proximity are available [15,75,79].

Collectively, these results and observations allow us to explain the NO oxidation activity specific to our AIE and SSIE samples. As we alluded to prior, NO oxidation activity in these samples is governed by complex contributions from multi-nuclear Cu species (e.g., CuO) and active Cu-dimers that durably reside in the catalyst. The AIE samples contain little of the former, and thus NO oxidation activity in these samples is dictated by the latter. For SiAl = 6 or 12, although isolated Cu content is highest among these samples, their inferior performance results from the tendency of active Cu-dimers in these samples to facilely split back to inactive isolated Cu-ions (high densities of residual Brønsted acid sites). SiAl = 18 and 24 contain the largest amount of isolated Cu in the form of $ZCu^{II}OH$, but they appear to differ in the fraction of suitable proximal isolated Cu for Cu-dimer formation that does not facilely decompose to isolated Cu-ions. In contrast, Cu-30 and Cu-36 contain similar amounts of isolated Cu in the form of $ZCu^{II}OH$ at what appears to be similar suitable proximity for NO oxidation, and thus resulting in analogous performance. It is worth noting that the ideal proximity of isolated Cu for NO oxidation appears to be achieved at Si/Al ~30. The SSIE samples contain varying amount of multi-nuclear Cu species that impact performance along with active Cu-dimers. Cu-6 s and Cu-12 s do not contain significant amounts of these, and thus their inferior performance is in line with Cu-6 and Cu-12 described above. Cu-18 s and Cu-24 s contain less total $ZCu^{II}OH$ versus their AIE counterparts, but the multi-nuclear Cu species in these samples yields similar NO oxidation performance. Finally, Cu-30 s and Cu-36 s, which contain similar amounts of $ZCu^{II}OH$ to Cu-24 s but notably less than their AIE counterparts, exhibit NO oxidation activity superior to all the other catalysts that can be directly attributed to the multi-nuclear Cu species in these catalysts.
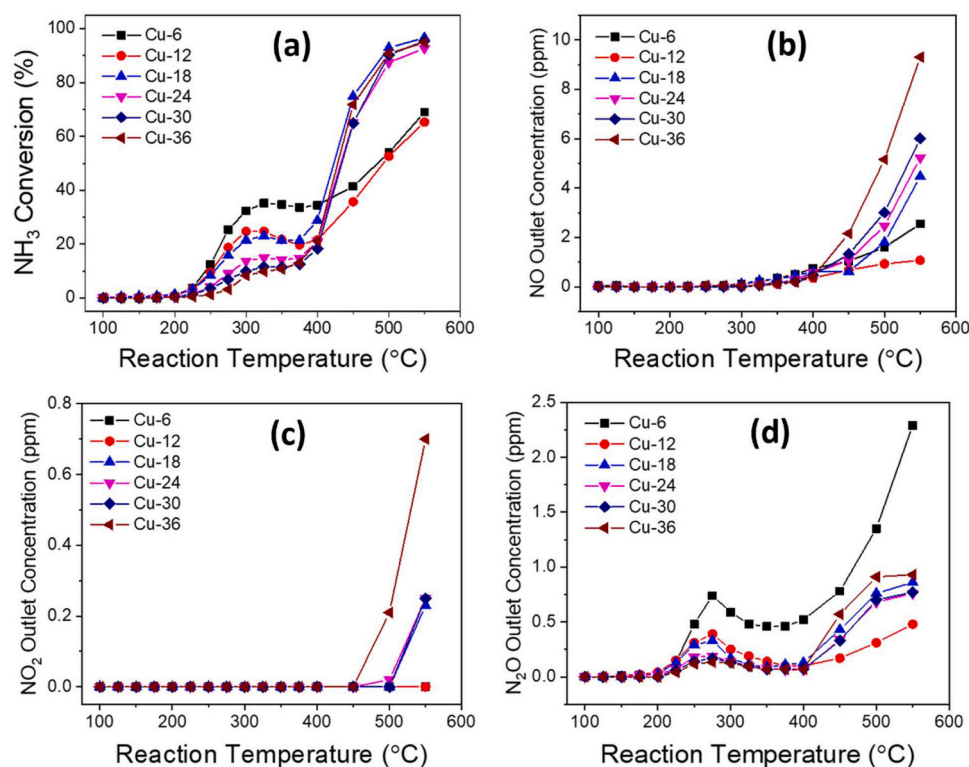
3.3. NH₃ oxidation

NH₃ oxidation performance over the AIE samples is presented in Fig. 4, including light-off curves in Fig. 4a and the formation of side products NO, NO₂ and N₂O in Figs. 4b-4d, respectively. In the light-off curves, all AEI samples display two distinct kinetic regimes. In the low temperature regime from ~200 to ~375 °C, NH₃ conversion first increases with increasing temperature, and then maintains largely invariant (or slightly decreases) with further increase of reaction temperature. In the high temperature regime above ~375 °C, NH₃ conversion increases with increasing temperature over all samples, however the temperature dependence is more pronounced for samples with Si/Al ≥ 18. Regarding the formation of NO, NO₂ and N₂O side products on the AEI catalysts, a few points are worth noting regarding these data. First, the yields of the side products are rather minor; even at a reaction temperature of 550 °C, the combined selectivity to these molecules is less than 4%. Second, the formation of these side products also follows clear dependence on reaction temperature and support Si/Al ratio. For example, NO and N₂O formation is observed in both low and high temperature regimes on all catalysts, but NO₂ formation is only found in the high temperature regime, and only on catalysts with Si/Al ≥ 18. Results for the same measurements on the SSIE samples are shown in Fig. S6. These samples also display two distinct kinetic regimes below and above ~375 °C, and similar side product formation dependences on temperature and support Si/Al ratio.

It is demonstrated in literature that standard NH₃-SCR over Cu/CHA also displays two distinct kinetic regimes below ~250 °C and above ~350 °C. It has been well documented that SCR occurs on (i) NH₃-solved, mobile Cu active sites in the low temperature regime, and (ii) immobilized Cu active sites no longer containing permanent NH₃ ligands in the high temperature regime [13,14,16]. Within the temperature window where these two regimes overlap (250–350 °C), "bizarre" kinetic behavior is often observed, e.g., NOx conversion decreases with increasing temperature (termed the 'seagull' shape), that has been attributed to gradual Cu immobilization [16,18]. Based on such prior knowledge, we suggest a similar active site transition for NH₃ oxidation over Cu-ions, i.e., it occurs on NH₃-solvated Cu-ions below ~300 °C but immobilized Cu above ~400 °C; between these two temperatures, the two kinetic regimes overlap. It is important to note that CuO clusters of varying sizes are also active for NH₃ oxidation. Therefore, an overall picture of possible reaction mechanisms and Cu site requirements of the two kinetic regimes can only be obtained by examining both the AIE samples (Cu-ion dominant) and the SSIE samples (with both Cu-ion and CuO) within a wide reaction temperature range.

The NH₃ light-off data in Fig. 4a and S6a were normalized to rates (mole NH₃ mole$_{Cu}^{-1}$ s^{-1}) with respect to total Cu loading, and the resultant data were subjected to Arrhenius analysis. Figs. 5a and 5b present results for the AIE and SSIE samples, respectively. For both low- and high-temperature kinetic regimes, apparent activation energies were calculated using the portion of data displaying linear Arrhenius behavior, and the results are tabulated in the figures.

We first discuss the low-temperature regime. Among the AIE samples, Cu-6 displays an Ea of ~120 kJ/mol, Cu-12 displays an Ea of ~100 kJ/mol, and the other samples show largely invariant Ea values of ~70–80 kJ/mol. Note that for standard NH₃-SCR, low-temperature regime Ea values are typically found within ~40–85 kJ/mol depending on the relative rate-controlling from the reduction and oxidation halves of the redox cycling [22]. As such, NH₃ oxidation over the AIE samples, in particular Cu-6 and Cu-12, clearly display higher barriers for reactant activation as compared to standard NH₃-SCR. Over the SSIE catalysts, low-temperature NH₃ oxidation Ea values, except that of Cu-6 s, are also substantially higher than low-temperature standard NH₃-SCR Ea values reported in literature. Overall, from the simple Ea comparison between standard NH₃-SCR and NH₃ oxidation, the latter reaction displays higher activation barriers attributable to NH₃ activation, which could be either the formation of hydrazine (i.e., the

Fig. 4. Steady state NH_3 oxidation reaction results over the AIE catalysts. (**a**) NH_3 conversion vs. temperature plots; (**b**) NO outlet vs. temperature; (**c**) NO_2 outlet vs. temperature; (**d**) N_2O outlet vs. temperature. 120 mg catalyst was used; reactant composition included 380 ppm NH_3, 10% O_2, ~2.5% H_2O, and balanced N_2; the total flow rate was 600 ml/min, and the gas hourly space velocity (GHSV) was estimated to be 200,000 h^{-1}.

hydrazine mechanism), or NH_3 oxidation to NO (i.e., the i-SCR mechanism). However, it is our belief that the i-SCR mechanism is more consistent with the Ea value trends observed here. For example, both Cu-6 and Cu-6 s contain primarily Z_2Cu^{II} but NH_3 oxidation Ea values are rather different for the two samples. Such a difference is difficult to justify from the hydrazine mechanism, but is readily explained with the i-SCR mechanism, that is, the lower Ea for Cu-6 s can be due mainly to its lower isolated Cu-ion content which triggers stronger rate-controlling from the oxidation half cycle [22]. Following the same rationale, it is also important to realize that for the SSIE samples, CuO clusters also play important roles in the low-temperature regime. Note that isolated Cu-ion content for this series of samples decreases with increasing Si/Al ratio (Table 1); if Cu-ions are the only active sites for the reaction, it is anticipated that Ea values should decrease with increasing Si/Al ratio. The very high Ea values found for the high Si/Al ratio SSIE samples can only be rationalized such that activation barriers for NH_3 oxidation to NO over CuO clusters are higher than those over isolated Cu-ions. Next, we show that the formation of side products is also consistent with the i-SCR mechanism.

In the low temperature regime for all samples (AIE and SSIE), NO is barely detected in the effluent (Fig. 4b, S6b). This finding is consistent with prior proposals that NH_3-SCO follows the i-SCR mechanism, that is, NO is rapidly consumed by the SCR reaction upon its formation [7–9]. The formation of N_2O in this regime (Fig. 4d, S6d), which displays an interesting volcano line shape as a function of temperature (N_2O yield shows a local maximum at ~275 °C), is another piece of evidence supporting the i-SCR mechanism. It is well known that N_2O formation during low temperature standard SCR displays a similar volcano line shape [24,80,81]. Even though the N_2O formation mechanism during SCR over Cu/CHA is still heavily debated, and while some favor an NH_4NO_3 decomposition mechanism whereas others suggest other intermediates [24, 81–89], no literature ever reported that N_2O is associated with a hydrazine intermediate. It is also interesting to note from

Fig. 4d that N_2O formation on Cu-6 is comparatively high versus the other samples. Since extra framework Al content in zeolites increases with decreasing Si/Al ratio [31], it is possible that the excess N_2O is formed on Cu-aluminate minor sites on Cu-6. This is supported by Deka et al. [90] who, in studying SCR over Cu catalysts formed by different methods, discovered that such sites are particularly selective toward N_2O formation.

Since the i-SCR mechanism requires that the Cu sites catalyze NH_3 oxidation in a cascade manner, i.e., NH_3 oxidation to NO followed by NO reduction by NH_3, and also since both isolated Cu-ions and CuO clusters contribute to the overall chemistry, it is useful to compare Cu atomic efficiency among the catalysts. We chose two representative reaction temperatures to compare NH_3 conversion rates, 275 °C and 450 °C, and the comparisons are shown in Fig. 6. We first focus on 275 °C, with the results shown in Figs. 6a and 6b for the AIE and SSIE samples, respectively. As Fig. 6a shows for the AIE samples, Cu atomic efficiency at 275 °C follows the order Cu-12 ≈ Cu-18 > Cu-24 > Cu-30 ≈ Cu-6 > Cu-36. Regarding the NH_3 oxidation to NO step, it is safe to presume that redox active $ZCu^{II}OH$ is more active than redox resistant Z_2Cu^{II} which has been confirmed by prior H_2 and NH_3 titration studies [78,91]. Regarding the standard SCR step, prior DFT calculations revealed that reaction activation energies over NH_3 solvated Z_2Cu^{II} and $ZCu^{II}OH$ are similar [15]. It has also been reported that Z_2Cu^{II} undergoes facile hydrolysis to $ZCu^{II}OH$ under low temperature SCR conditions [21]. As such, standard SCR kinetics should not be strongly influenced by Cu-ion speciation. However, standard SCR kinetics is indeed strongly influenced by Cu-ion concentration, where Cu atomic efficiency increases with increasing Cu-ion concentration [22]. Based on such prior understandings, we suggest that the somewhat inferior Cu atomic efficiency for Cu-6 at 275 °C (versus Cu-12 and Cu-18) is due to the fact that some Z_2Cu^{II} species in this catalyst resist facile hydrolysis to $ZCu^{II}OH$ and are therefore not active for NH_3 oxidation to NO. On the other hand, the monotonic Cu atomic efficiency decrease from Cu-18 to Cu-36 is
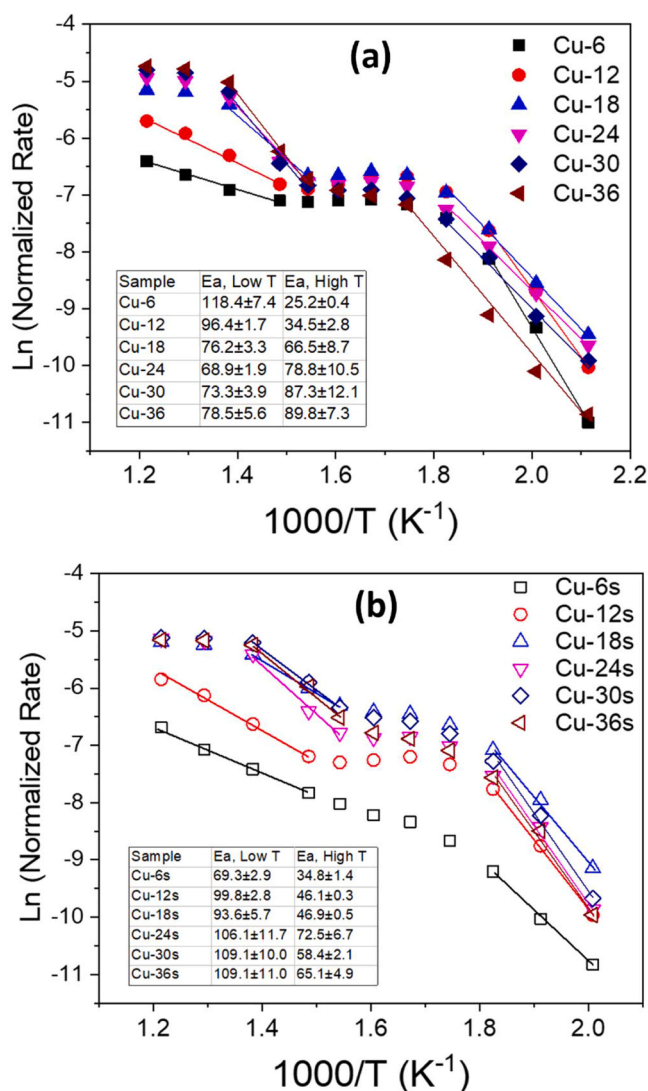
Fig. 5. Arrhenius plots derived using NH$_3$ conversion data shown in Fig. 4a and S6a. (**a**) AIE samples, (**b**) SSIE samples. Apparent reaction activation energies for both low and high temperature regimes are tabulated within the plots.

likely due to reduced Cu-ion concentration. This follows since these latter samples contain primarily ZCu^{II}OH (Table S3) and are arguably equally active in catalyzing NH$_3$ oxidation to NO. However, since total Cu-ion concentrations decrease with increasing Si/Al ratio (Table 1), the subsequent NO reduction step becomes progressively less efficient as Si/Al ratio rises. For the SSIE samples shown in Fig. 6b, two points are worth noting. First, the Cu atomic efficiency of Cu-6 s is exceedingly low confirming our notion above that Z$_2$Cu^{II} species does not hydrolyze facilely to ZCu^{II}OH at SiAl = 6; as such, the NH$_3$ oxidation to NO step becomes inhibited. Second, Cu-30 s and Cu-36 s display even higher Cu atomic efficiency than Cu-12 and Cu-18. Note that these 4 samples possess similar total Cu contents, however Cu-30 s and Cu-36 s contain substantially higher CuO cluster contents than Cu-12 and Cu-18. This thus provides prevailing evidence that CuO clusters indeed play important roles for the low-temperature regime. Since CuO clusters are not active for SCR, their contribution to the NH$_3$ oxidation cascade must be to facilitate the NH$_3$ oxidation to NO step. As such, our data here confirms a synergy between isolated Cu-ions and CuO clusters for low-temperate NH$_3$ oxidation which appears to be inherent in the i-SCR mechanism.

Next, we turn our attention to the high-temperature regime (450 °C), with the Cu atomic efficiency results shown in Figs. 6c and 6d for the AIE

and SSIE samples, respectively. The results show that Cu-6 and Cu-6 s exhibit the lowest Cu atomic efficiency, followed by Cu-12 and Cu-12 s, whereas other samples display similar Cu atomic efficiency. To explain these results, it is useful to first note that at such high temperatures, an NH$_3$ solvation effect is no longer functional, i.e., Cu-ions are now immobilized at CHA framework windows by coordinating to lattice oxygen [14–16]. As Figs. 5a and 5b show, Cu-6, Cu-12 and Cu-6 s display high temperature NH$_3$ conversion Ea values that are considerably lower than other samples. Furthermore, these samples also display the lowest Ea values for dry NO oxidation as shown in Figs. 3a and 3b. For the other samples, the trend of NO oxidation Ea versus Si/Al ratio is fairly consistent with NH$_3$ oxidation Ea versus Si/Al ratio. Such similarity between these two reactions suggests that they largely share the same active Cu sites, i.e., for samples that contain primarily isolated Cu-ions, in situ Cu-dimers formed from ZCu^{II}OH are the major active sites; for samples that contain both isolated Cu-ions and large quantities of CuO clusters, NH$_3$ oxidation is sustained by both in situ Cu-dimers and CuO clusters. Furthermore, Cu-dimers balanced by framework Al of the close proximities offer more facile NH$_3$ oxidation than Cu-dimers balanced by framework Al farther apart, and the latter species display NH$_3$ oxidation properties similar to larger CuO clusters. Thus, to summarize, the results shown in Figs. 6c and 6d are rationalized by the low stability of Cu-dimers at elevated temperatures in samples with low Si/Al ratios. In other words, even though the Cu-dimers balanced by framework Al of the close proximities offer high activity (i.e., low Ea), their low densities at low Si/Al ratios precludes high Cu atomic efficiency on the total Cu basis.

Finally, the formation of side products NO, NO$_2$ and N$_2$O are compared between the two series of catalysts in the high-temperature regime (Figs. 4b – 4d and Fig. S6b – S6d). For both series of catalysts, side product yields increase with increasing support Si/Al ratio; between the two series, SSIE samples typically display higher side product yields as compared to the AIE samples with the same Si/Al ratio. Such trends demonstrate that in situ Cu-dimers and permanent CuO clusters are not 100% selective in catalyzing NH$_3$ oxidation to NO, leading to the formation of small quantities of NO$_2$ and N$_2$O. Furthermore, CuO clusters appear to be less selective than Cu-dimers.

3.4. DFT calculations

NO oxidation on Cu/CHA has been studied in detail in the past via DFT calculations [45]. As such, we only focus on NH$_3$ oxidation here. As discussed above, our reaction kinetics data suggest that low temperature NH$_3$ oxidation on Cu/CHA occurs on NH$_3$-solvated ZCu^{II}OH (i.e., Cu^{II}(NH$_3$)$_3$OH), and follows the i-SCR mechanism. To provide in-depth understanding of the i-SCR mechanism, we calculated energetics of both NH$_3$ oxidation (by O$_2$) to NO, and standard SCR on Cu^{II}(NH$_3$)$_3$OH. Fig. 7a summarizes the proposed reaction schemes for both pathways, and Fig. 7b presents the corresponding energy diagrams. For NH$_3$ oxidation (by O$_2$) to NO, we propose that NH$_3$ activation in the first step is achieved by -OH assisted N-H bond cleavage resulting in the formation of a -NH$_2$ intermediate (and H$_2$O). Following this, the -NH$_2$ intermediate is oxidized by O$_2$ to NO and H$_2$O, and concurrently the Cu center is reduced to Cu^{I}(NH$_3$)$_2$. For the reduction half cycle of standard SCR, we propose -OH assisted NO activation to HONO as suggested previously [16,92], followed by NH$_3$ interaction with HONO to a highly unstable nitrite intermediate that readily decomposes to N$_2$ and H$_2$O, and the reduction of the Cu center to Cu^{I}(NH$_3$)$_2$. The common Cu^{I}(NH$_3$)$_2$ intermediate of the two reactions is oxidized back to a common Cu$_2^{II}$(NH$_3$)$_2$O$_2$ intermediate [16,19]. Even though the reactions shown in Fig. 7a are only part of the reaction steps for the complete catalytic turnovers, we believe that these are the most important steps.

From the energy diagrams shown in Fig. 7b, endergonic steps found for NH$_3$ oxidation by O$_2$ to NO (green line) include: (i) the first N-H bond cleavage step with $\Delta H_{rxn} = 0.35$ eV, (ii) the separation of H$_2$O from Cu^{II}(NH$_3$)$_2$NH$_2$ with $\Delta H_{rxn} = 0.33$ eV, and (iii) the NO desorption of
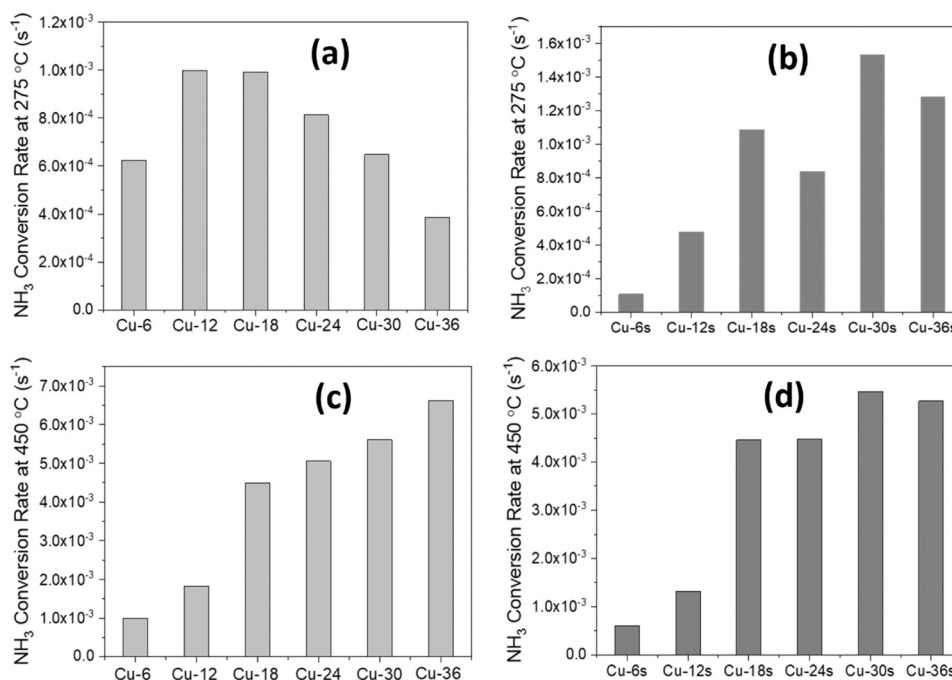
Fig. 6. NH$_3$ conversion rate comparison for (**a**) AIE samples, 275 °C; (**b**) SSIE samples, 275 °C; (**c**) AIE samples, 450 °C; (**b**) SSIE samples, 450 °C.
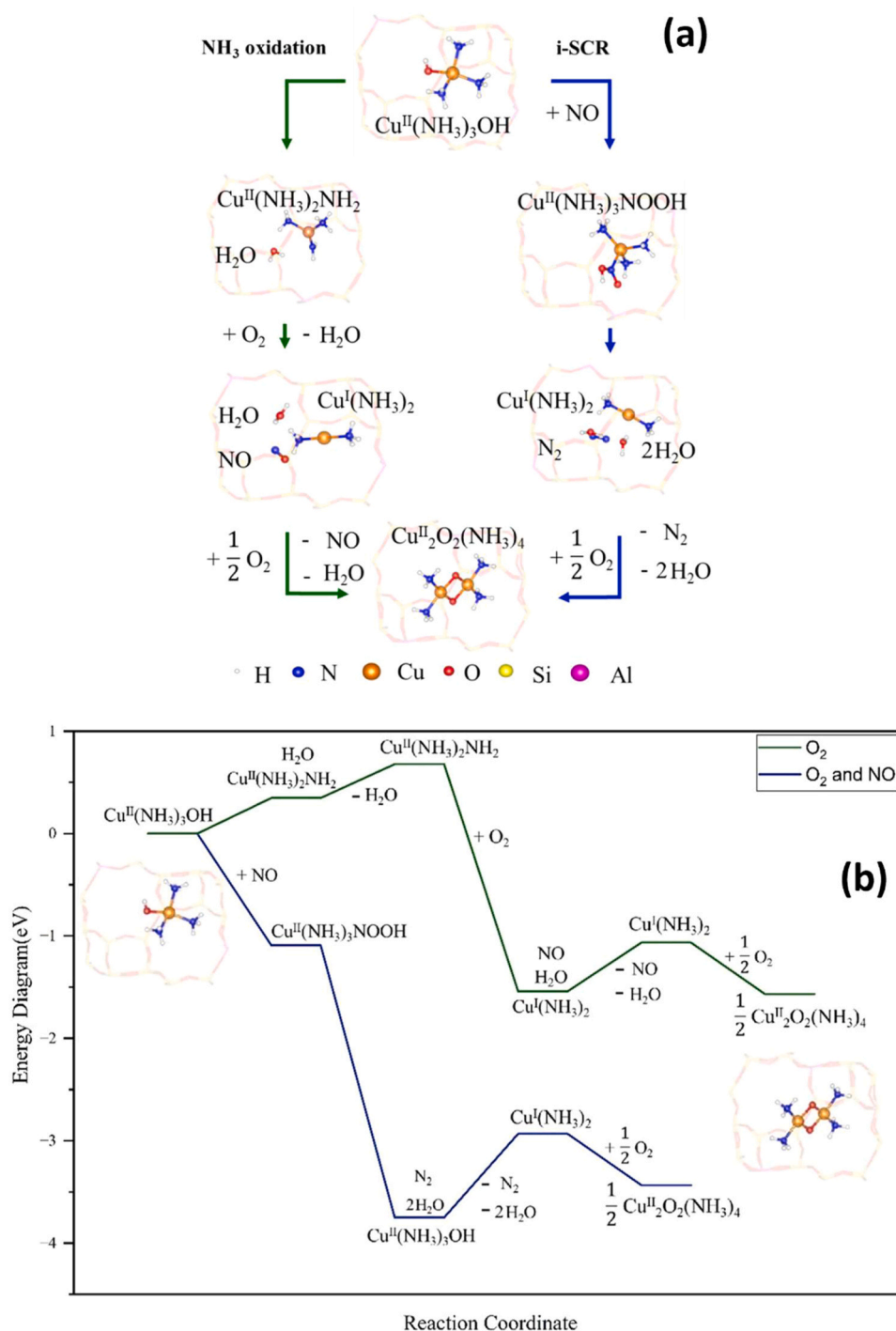
0.15 eV and H$_2$O desorption of 0.33 eV following the formation of the Cu^I(NH$_3$)$_2$ intermediate. In contrast, the endergonic steps found during standard SCR (blue line) is the desorption of N$_2$ of 0.11 eV and two H$_2$O desorption of 0.33 eV and 0.39 eV following the formation of the same Cu^I(NH$_3$)$_2$ intermediate. As such, these data clearly demonstrate that NH$_3$ oxidation by O$_2$ to NO is energetically more demanding than SCR, and this agrees with the fact that over the same Cu-zeolite catalyst, NH$_3$ oxidation typically lights off at higher temperatures than standard SCR [32,71]. Also, the choice of the i-SCR mechanism for NH$_3$ oxidation is readily justified by the fact that, in the presence of NO, the endergonic N-H bond activation is avoided. More details regarding Fig. 7 are shown in the Supporting Information, including adsorption energies in Table S6, reaction energies in Table S7, and bader charge analysis of Cu atoms in Table S8. We also acknowledge that the energetics of NH$_3$ oxidation over Cu/CHA will be influenced by the exchange-correlation functionals, such as GGA-PBE and hybrid HSE06 [15,17]. However, we expect that the choice of functional will not change the main conclusion derived from Fig. 7 that NH$_3$ activation by NO+O$_2$ (i-SCR) is energetically more favorable than that with O$_2$ alone.

In the high temperature regime, our experimental results suggest that immobilized Cu-dimers are the active sites for NH$_3$ oxidation, and the most stable Cu-dimers are located within the chabazite cage but not within the same 6- or 8-membered rings. Therefore, in Fig. 8**a** we simulated dimerization of two ZCu^{II}OH, each located next to an 8-membered ring of the same chabazite cage, to a double-bridged ZCu^{II}-(OH)$_2$-Cu^{II}Z. This reaction is slightly endergonic with $\Delta H_{rxn} = 0.07$ eV. To elucidate if this complex is active for NH$_3$ oxidation, in Fig. 8**b** we calculated NH$_3$ activation via N-H bond cleavage to -NH$_2$ on this complex. The results show that this reaction is highly endergonic with $\Delta H_{rxn} = 1.54$ eV. As such, it is highly unlikely that ZCu^{II}-(OH)$_2$-Cu^{II}Z serves as the active site for high temperature NH$_3$ oxidation. In this regard, we further calculated ZCu^{II}-(OH)$_2$-Cu^{II}Z dehydration to single-bridged ZCu^{II}-O-Cu^{II}Z, and NH$_3$ activation via N-H bond cleavage on this latter complex, with the results are shown in Figs. 8**c** and 8**d**, respectively. ZCu^{II}-O-Cu^{II}Z formation is exergonic with a reaction energy of -0.53 eV, and NH$_3$ activation is still endergonic but the reaction energy drops to 0.89 eV. From these calculations, it can be readily concluded that ZCu^{II}-O-Cu^{II}Z is a more likely active center for high temperature

NH$_3$ oxidation. However, we would like to point out that our simulations of Cu-dimer active sites are far from exhaustive. For example, a double-bridged ZCu^{II}-O$_2$-Cu^{II}Z may also be a catalytically relevant intermediate here [78].

We also made some other calculations, e.g., additional ZCu^{II}OH pair configurations within the chabazite framework, NH$_3$ and -NH$_2$ adsorption site and energies; the results are shown in Figs. S7 to S10. First, Fig. S7 demonstrates that alternate ZCu^{II}OH paired configurations versus those occurring next to an 8-membered ring of the same chabazite cage are slightly more endergonic and thus not favorable, but not significantly impactful. This suggests that varied ZCu^{II}OH paired configurations are certainly feasible. Next, to confirm our conclusion above regarding the highly unlikely role of double-bridged ZCu^{II}-(OH)$_2$-Cu^{II}Z in high temperature NH$_3$ oxidation, in Fig. S1 and Fig. S9 we assess alternate starting and ending configurations of NH$_3$ activation (i.e., NH$_3$ adsorption, NH$_2$ adsorption), respectively, on double-bridged ZCu^{II}-(OH)$_2$-Cu^{II}Z. The results show no significant impact of configuration on the highly endergonic nature of N-H bond cleavage on double-bridged ZCu^{II}-(OH)$_2$-Cu^{II}Z, thus confirming its unlikely role in high temperature NH$_3$ oxidation. And last, further confirming the likely role of single-bridged ZCu^{II}-O-Cu^{II}Z, for NH$_3$ activation, Fig. S10 compares alternate configurations of NH$_3$ adsorption on ZCu^{II}-O-Cu^{II}Z and shows that different configurations less exergonic than what is proposed as the starting intermediate in Fig. 8**d**. Collectively, these results support the determination that ZCu^{II}-O-Cu^{II}Z is the likely active center for high temperature NH$_3$ oxidation on these catalysts.

Finally, we note that samples with Si/Al ratios of 6 and 12, i.e., Cu-6, Cu-6 s, Cu-12 and Cu-12 s, offer the lowest high temperature NH$_3$ oxidation efficiency (Fig. 4**a**, Fig. S6a). Interestingly, these samples do not catalyze NH$_3$ deep oxidation to NO$_2$ at all at 550 °C (Fig. 4**c**, Fig. S6c), suggesting their negligible contents of stable Cu-dimers and CuO clusters. As such, it is likely that isolated Cu-ions, in particular Z$_2$Cu^{II}, sustain at least a portion of high temperature NH$_3$ oxidation activity in these samples. From the rate comparison plots shown in Fig. 5, isolated Cu-ions are clearly much less active than Cu-dimers and CuO clusters. This is consistent with DFT calculated NH$_3 \rightarrow$ -NH$_2$ energy of 1.23 eV on Z$_2$Cu^{II} [93]. We note also that Cu-dimers and CuO clusters are most certainly more active than isolated Cu-ions in O$_2$ activation.

Fig. 7. The proposed schemes (**a**) and the DFT electronic energy diagrams (**b**) of NH_3 oxidation over NH_3-solved $ZCu^{II}OH$ via the i-SCR mechanism. Color code: H (white), N (blue), Cu (orange), O (red), Si (blue), Al (pink).
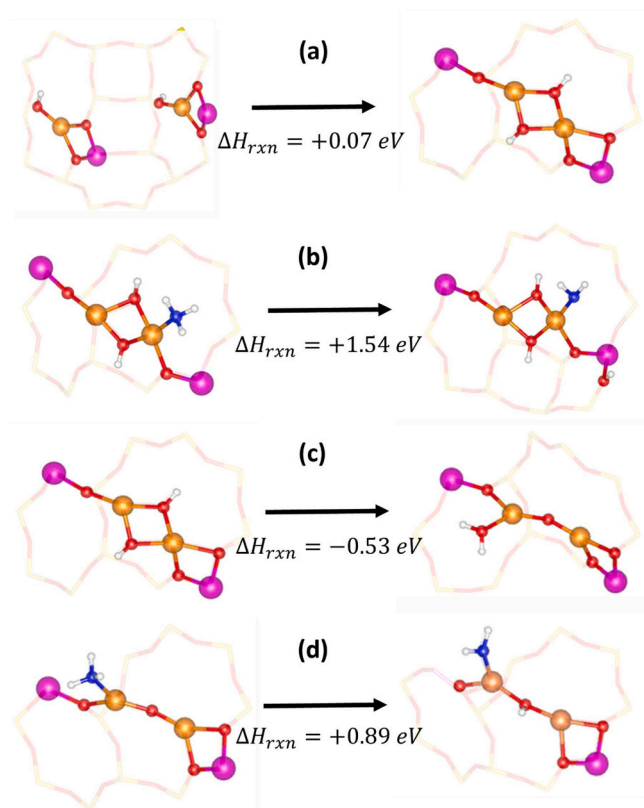
Such calculations, however, are beyond the scope of the current work.

4. Conclusions

To reveal NO and NH_3 oxidation mechanisms and site requirements on Cu/CHA, two series of Cu/CHA catalysts are synthesized via AIE and SSIE, using SSZ-13 supports of varying Si/Al ratios. The AIE samples contain primarily isolated Cu-ions, where Z_2Cu^{II} vs. $ZCu^{II}OH$ speciation systemically varies with Si/Al ratio. For the SSIE samples, population of isolated Cu-ions and CuO clusters also varies with Si/Al ratio. As such, these catalysts cover a wide range of Cu speciation and enable NO and NH_3 oxidation structure-activity correlations to be readily probed via a combination of Cu speciation quantification with H_2-TPR, and reaction kinetics. NO oxidation on these catalysts occurs on multinuclear Cu sites, including in situ Cu-dimers formed from $ZCu^{II}OH$ dimerization and permanent CuO clusters present in the as-synthesized catalysts. In situ Cu-dimers balanced by framework Al in close proximity appear more active than Cu-dimers balanced by framework Al that are farther apart. However, the former dimers are less stable than the latter and exhibit more facile decomposition back to isolated Cu-ions that are not active for NO oxidation.

NH_3 oxidation follows an internal SCR (i-SCR) mechanism and

Fig. 8. The potential configurations and the associated formation energetics to generate the ZCu^{II}-(OH)$_2$-Cu^{II}Z (**a**) and ZCu^{II}-O-Cu^{II}Z (**c**), from ZCu^{II}OH. The first N-H bond cleavage reaction energy of NH$_3$ over ZCu^{II}-(OH)$_2$-Cu^{II}Z (**b**) and ZCu^{II}-O-Cu^{II}Z (**d**).

displays unique kinetic behavior below ~300 °C and above ~400 °C. NH$_3$-solvated mobile Cu^{II}(NH$_3$)$_3$OH species are active for NH$_3$ oxidation at low-temperature, and the same species also catalyze further reduction of NO (produced from NH$_3$ oxidation) to N$_2$ and H$_2$O. Furthermore, our results show that permanent CuO clusters also contribute to low temperature activity by catalyzing NH$_3$ oxidation to NO, and here we confirm a synergy between isolated Cu-ions and CuO clusters for low-temperate NH$_3$ oxidation which appears to be inherent in the i-SCR mechanism. In the high-temperature regime, active Cu sites for NH$_3$ oxidation to NO are in situ Cu-dimers and permanent CuO clusters (similar to dry NO oxidation), whereas isolated Cu-ions (immobilized at high temperature) sustain selective NO reduction by NH$_3$. Via DFT, i-SCR pathways, including NH$_3$ oxidation to NO, and the subsequent standard SCR, are calculated. The results confirm the feasibility of the i-SCR mechanism. ZCu^{II}OH dimerization pathways, and how NH$_3$ is activated on such dimers, are also calculated. DFT results suggest that ZCu^{II}-O-Cu^{II}Z is a much more plausible active site for high temperature NH$_3$ oxidation than ZCu^{II}-(OH)$_2$-Cu^{II}Z.

CRediT authorship contribution statement

Wang Yong: Supervision, Project administration, Methodology, Funding acquisition, Conceptualization. **Rappe Kenneth:** Writing – review & editing, Writing – original draft, Supervision, Project administration, Funding acquisition, Formal analysis. **Gao Feng:** Writing – review & editing, Writing – original draft, Supervision, Project administration, Methodology, Investigation, Formal analysis, Conceptualization. **Che Fanglin:** Writing – review & editing, Writing – original draft, Supervision, Project administration, Methodology, Funding acquisition, Formal analysis, Conceptualization. **Wang Yilin:** Writing – original draft, Investigation, Formal analysis. **Zhao Runze:** Writing – review &

editing, Writing – original draft, Software, Methodology, Investigation, Formal analysis, Conceptualization.

Declaration of Competing Interest

The authors declare that they have no known competing financial interests or personal relationships that could have appeared to influence the work reported in this paper.

Data Availability

Data will be made available on request.

Author Contributions

F.G. designed the experimental part of the project and F.C. designed the theoretical part of the project. F.G., K.G.R., Y.W. and F.C. supervised the project. Y.L.W. and F.G. carried out experiment measurements and materials characterizations. R.Z. carried out DFT calculations and analyzed data. F.G., K.G.R., R.Z., and F.C co-wrote the paper. All authors discussed the results and contributed to the preparation of the manuscript.

Appendix A. Supporting information

Supplementary data associated with this article can be found in the online version at doi:10.1016/j.apcatb.2024.123726.

References

[1] G. Busca, L. Lietti, G. Ramis, F. Berti, Chemical and mechanistic aspects of the selective catalytic reduction of NOx by ammonia over oxide catalysts: a review, Appl. Catal. B-Environ. 18 (1998) 1–36.

[2] L.P. Han, S.X. Cai, M. Gao, J. Hasegawa, P.L. Wang, J.P. Zhang, L.Y. Shi, D.S. Zhang, Selective catalytic reduction of NOx with NH3 by using novel catalysts: state of the art and future prospects, Chem. Rev. 119 (2019) 10916–10976.

[3] A.M. Beale, F. Gao, I. Lezcano-Gonzalez, C.H.F. Peden, J. Szanyi, Recent advances in automotive catalysis for NOx emission control by small-pore microporous materials, Chem. Soc. Rev. 44 (2015) 7371–7405.

[4] Z.L. Chen, W. Song, C.C. Hu, X.J. Liu, G.Y. Chen, W.W. Walters, G. Michalski, C.Q. Liu, D. Fowler, X.Y. Liu, Significant contributions of combustion-related sources to ammonia emissions, Nat. Commun. 13 (2022) 7710.

[5] A. Scheuer, W. Hauptmann, A. Drochner, J. Gieshoff, H. Vogel, M. Votsmeier, Dual layer automotive ammonia oxidation catalysts: Experiments and computer simulation, Appl. Catal. B-Environ. 111 (2012) 445–455.

[6] S. Shrestha, M.P. Harold, K. Kamasamudram, A. Yezerets, Ammonia oxidation on structured composite catalysts, Top. Catal. 56 (2013) 182–186.

[7] M. Jablonska, R. Palkovits, Copper based catalysts for the selective ammonia oxidation into nitrogen and water vapour-Recent trends and open challenges, Appl. Catal. B-Environ. 181 (2016) 332–351.

[8] M. Jablonska, Progress on selective catalytic ammonia oxidation (NH3-SCO) over Cu-containing zeolite-based catalysts, Chemcatchem 12 (2020) 4490–4500.

[9] R.Q. Long, R.T. Yang, Selective catalytic oxidation (SCO) of ammonia to nitrogen over Fe-exchanged zeolites, J. Catal. 201 (2001) 145–152.

[10] T. Zhang, H.Z. Chang, Y.C. You, C.N. Shi, J.H. Li, Excellent activity and selectivity of one-pot synthesized Cu SSZ-13 catalyst in the selective catalytic oxidation of ammonia to nitrogen, Environ. Sci. Technol. 52 (2018) 4802–4808.

[11] W.J. Liu, Y.F. Long, S.N. Liu, Y.Y. Zhou, X. Tong, Y.J. Yin, X.Y. Li, K. Hu, J.J. Hu, Commercial SCR catalyst modified with different noble metals (Ag, Pt, Pd) to efficiently remove slip ammonia and NOx in the flue gas, J. Taiwan Inst. Chem. E 138 (2022).

[12] F. Gao, E.D. Walter, E.M. Karp, J.Y. Luo, R.G. Tonkyn, J.H. Kwak, J. Szanyi, C.H. F. Peden, Structure-activity relationships in NH3-SCR over Cu-SSZ-13 as probed by reaction kinetics and EPR studies, J. Catal. 300 (2013) 20–29.

[13] F. Gao, E.D. Walter, M. Kollar, Y.L. Wang, J. Szanyi, C.H.F. Peden, Understanding ammonia selective catalytic reduction kinetics over Cu/SSZ-13 from motion of the Cu ions, J. Catal. 319 (2014) 1–14.

[14] K.A. Lomachenko, E. Borfecchia, C. Negri, G. Berlier, C. Lamberti, P. Beato, H. Falsig, S. Bordiga, The Cu-CHA deNO(x) catalyst in action: temperature-dependent nh3-assisted selective catalytic reduction monitored by operando XAS and XES, J. Am. Chem. Soc. 138 (2016) 12025–12028.

[15] C. Paolucci, A.A. Parekh, I. Khurana, J.R. Di Iorio, H. Li, J.D.A. Caballero, A. J. Shih, T. Anggara, W.N. Delgass, J.T. Miller, F.H. Ribeiro, R. Gounder, W. F. Schneider, Catalysis in a cage: condition-dependent speciation and dynamics of exchanged Cu cations in SSZ-13 zeolites, J. Am. Chem. Soc. 138 (2016) 6028–6048.

[16] F. Gao, D.H. Mei, Y.L. Wang, J. Szanyi, C.H.F. Peden, Selective catalytic reduction over Cu/SSZ-13: linking homo- and heterogeneous catalysis, J. Am. Chem. Soc. 139 (2017) 4935–4942.

[17] C. Paolucci, I. Khurana, A.A. Parekh, S.C. Li, A.J. Shih, H. Li, J.R. Di Iorio, J. D. Albarracin-Caballero, A. Yezerets, J.T. Miller, W.N. Delgass, F.H. Ribeiro, W. F. Schneider, R. Gounder, Dynamic multinuclear sites formed by mobilized copper ions in NOx selective catalytic reduction, Science 357 (2017) 898–903.

[18] A. Marberger, A.W. Petrov, P. Steiger, M. Elsener, O. Krocher, M. Nachtegaal, D. Ferri, Time-resolved copper speciation during selective catalytic reduction of NO on Cu-SSZ-13, Nat. Catal. 1 (2018) 221–227.

[19] C. Negri, T. Selleri, E. Borfecchia, A. Martini, K.A. Lomachenko, T.V.W. Janssens, M. Cutini, S. Bordiga, G. Berlier, Structure and reactivity of oxygen-bridged diamino dicopper(II) complexes in Cu-ion-exchanged chabazite catalyst for NH3-mediated selective catalytic reduction, J. Am. Chem. Soc. 142 (2020) 15884–15896.

[20] W.S. Hu, T. Selleri, F. Gramigni, E. Fenes, K.R. Rout, S.J. Liu, I. Nova, D. Chen, X. Gao, E. Tronconi, On the redox mechanism of low-temperature NH3-SCR over Cu-CHA: a combined experimental and theoretical study of the reduction half cycle, Angew. Chem. Int. Ed. 60 (2021) 7197–7204.

[21] W.S. Hu, U. Iacobone, F. Gramigni, Y. Zhang, X.X. Wang, S.J. Liu, C.H. Zheng, I. Nova, X. Gao, E. Tronconi, Unraveling the hydrolysis of Z(2)Cu(2+) to ZCu(2+) (OH)(-) and its consequences for the low-temperature selective catalytic reduction of NO on Cu-CHA catalysts, ACS Catal. 11 (2021) 11616–11625.

[22] Y.Q. Wu, Y. Ma, Y.L. Wang, K.G. Rappe, N.M. Washton, Y. Wang, E.D. Walter, F. Gao, Rate controlling in low-temperature standard NH3-SCR: implications from operando EPR spectroscopy and reaction kinetics, J. Am. Chem. Soc. 144 (2022) 9734–9746.

[23] Y. Qiu, C. Fan, C.C. Sun, H.C. Zhu, W.T. Yi, J.Z. Chen, L.Y. Guo, X.X. Niu, J.J. Chen, Y. Peng, T. Zhang, J.H. Li, New insight into the in situ SO2 poisoning mechanism over Cu-SSZ-13 for the selective catalytic reduction of NOx with NH3, Catalysts 10 (2020).

[24] B. Liu, D.W. Yao, F. Wu, L. Wei, X.W. Li, X.L. Wang, Experimental investigation on N2O formation during the selective catalytic reduction of NOx with NH3 over Cu-SSZ-13, Ind. Eng. Chem. Res 58 (2019) 20516–20527.

[25] X. Auvray, A. Grant, B. Lundberg, L. Olsson, Lean and rich aging of a Cu/SSZ-13 catalyst for combined lean NOx trap (LNT) and selective catalytic reduction (SCR) concept, Catal. Sci. Technol. 9 (2019) 2152–2162.

[26] S. Han, J. Cheng, C.K. Zheng, Q. Ye, S.Y. Cheng, T.F. Kang, H.X. Dai, Effect of Si/Al ratio on catalytic performance of hydrothermally aged Cu-SSZ-13 for the NH3-SCR of NO in simulated diesel exhaust, Appl. Surf. Sci. 419 (2017) 382–392.

[27] K. Wijayanti, K. Leistner, S. Chand, A. Kumar, K. Kamasamudram, N.W. Currier, A. Yezerets, L. Olsson, Deactivation of Cu-SSZ-13 by SO2 exposure under SCR conditions, Catal. Sci. Technol. 6 (2016) 2565–2579.

[28] J.Y. Luo, D. Wang, A. Kumar, J.H. Li, K. Kamasamudram, Identification of two types of Cu sites in Cu/SSZ-13 and their unique responses to hydrothermal aging and sulfur poisoning, Catal. Today 267 (2016) 3–9.

[29] K. Wijayanti, S. Andonova, A. Kumar, J.H. Li, K. Kamasamudram, N.W. Currier, A. Yezerets, L. Olsson, Impact of sulfur oxide on NH3-SCR over Cu-SAPO-34, Appl. Catal. B-Environ. 166 (2015) 568–579.

[30] D. Wang, Y. Jangjou, Y. Liu, M.K. Sharma, J.Y. Luo, J.H. Li, K. Kamasamudram, W. S. Epling, A comparison of hydrothermal aging effects on NH3-SCR of NOx over Cu-SSZ-13 and Cu-SAPO-34 catalysts, Appl. Catal. B-Environ. 165 (2015) 438–445.

[31] F. Gao, N.M. Washton, Y.L. Wang, M. Kollar, J. Szanyi, C.H.F. Peden, Effects of Si/Al ratio on Cu/SSZ-13 NH3-SCR catalysts: Implications for the active Cu species and the roles of Bronsted acidity, J. Catal. 331 (2015) 25–38.

[32] F. Gao, Y.L. Wang, M. Kollar, N.M. Washton, J. Szanyi, C.H.F. Peden, A comparative kinetics study between Cu/SSZ-13 and Fe/SSZ-13 SCR catalysts, Catal. Today 258 (2015) 347–358.

[33] F. Gao, E.D. Walter, N.M. Washton, J. Szanyi, C.H.F. Peden, Synthesis and evaluation of Cu/SAPO-34 catalysts for NH3-SCR 2: Solid-state ion exchange and one-pot synthesis, Appl. Catal. B-Environ. 162 (2015) 501–514.

[34] T. Yu, T. Hao, D.Q. Fan, J. Wang, M.Q. Shen, W. Li, Recent NH3-SCR mechanism research over Cu/SAPO-34 catalyst, J. Phys. Chem. C. 118 (2014) 6565–6575.

[35] T. Yu, D.Q. Fan, T. Hao, J. Wang, M.Q. Shen, W. Li, The effect of various templates on the NH3-SCR activities over Cu/SAPO-34 catalysts, Chem. Eng. J. 243 (2014) 159–168.

[36] D. Wang, L. Zhang, J.H. Li, K. Kamasamudram, W.S. Epling, NH3-SCR over Cu/SAPO-34 - Zeolite acidity and Cu structure changes as a function of Cu loading, Catal. Today 231 (2014) 64–74.

[37] O. Mihai, C.R. Widyastuti, S. Andonova, K. Kamasamudram, J.H. Li, S.Y. Joshi, N. W. Currier, A. Yezerets, L. Olsson, The effect of Cu-loading on different reactions involved in NH3-SCR over Cu-BEA catalysts, J. Catal. 311 (2014) 170–181.

[38] H.Y. Zhu, J.H. Kwak, C.H.F. Peden, J. Szanyi, In situ DRIFTS-MS studies on the oxidation of adsorbed NH3 by NOx over a Cu-SSZ-13 zeolite, Catal. Today 205 (2013) 16–23.

[39] T. Yu, J. Wang, M.Q. Shen, W. Li, NH3-SCR over Cu/SAPO-34 catalysts with various acid contents and low Cu loading, Catal. Sci. Technol. 3 (2013) 3234–3241.

[40] P.S. Metkar, M.P. Harold, V. Balakotaiah, Experimental and kinetic modeling study of NH3-SCR of NOx on Fe-ZSM-5, Cu-chabazite and combined Fe- and Cu-zeolite monolithic catalysts, Chem. Eng. Sci. 87 (2013) 51–66.

[41] N. Wilken, K. Wijayanti, K. Kamasamudram, N.W. Currier, R. Vedaiyan, A. Yezerets, L. Olsson, Mechanistic investigation of hydrothermal aging of Cu-Beta for ammonia SCR, Appl. Catal. B-Environ. 111 (2012) 58–66.

[42] S.J. Schmieg, S.H. Oh, C.H. Kim, D.B. Brown, J.H. Lee, C.H.F. Peden, D.H. Kim, Thermal durability of Cu-CHA NH3-SCR catalysts for diesel NOx reduction, Catal. Today 184 (2012) 252–261.

[43] C.H.F. Peden, J.H. Kwak, S.D. Burton, R.G. Tonkyn, D.H. Kim, J.H. Lee, H.W. Jen, G. Cavataio, Y.S. Cheng, C.K. Lambert, Possible origin of improved high temperature performance of hydrothermally aged Cu/beta zeolite catalysts, Catal. Today 184 (2012) 245–251.

[44] J.H. Kwak, D. Tran, J. Szanyi, C.H.F. Peden, J.H. Lee, The effect of copper loading on the selective catalytic reduction of nitric oxide by ammonia over Cu-SSZ-13, Catal. Lett. 142 (2012) 295–301.

[45] A.A. Verma, S.A. Bates, T. Anggara, C. Paolucci, A.A. Parekh, K. Kamasamudram, A. Yezerets, J.T. Miller, W.N. Delgass, W.F. Schneider, F.H. Ribeiro, NO oxidation: a probe reaction on Cu-SSZ-13, J. Catal. 312 (2014) 179–190.

[46] F. Goltl, S. Bhandari, M. Mavrikakis, Thermodynamics perspective on the stepwise conversion of methane to methanol over Cu-exchanged SSZ-13, ACS Catal. 11 (2021) 7719–7734.

[47] U. Engedahl, H. Gronbeck, A. Hellman, First-principles study of oxidation state and coordination of Cu-dimers in Cu-SSZ-13 during methane-to-methanol reaction conditions, J. Phys. Chem. C. 123 (2019) 26145–26150.

[48] L. Artiglia, V.L. Sushkevich, D. Palagin, A.J. Knorpp, K. Roy, J.A. van Bokhoven, In situ X-ray photoelectron spectroscopy detects multiple active sites involved in the selective anaerobic oxidation of methane in copper-exchanged zeolites, ACS Catal. 9 (2019) 6728–6737.

[49] Y.R. Cui, Y.L. Wang, D.H. Mei, E.D. Walter, N.M. Washton, J.D. Holladay, Y. Wang, J. Szanyi, C.H.F. Peden, F. Gao, Revisiting effects of alkali metal and alkaline earth co-cation additives to Cu/SSZ-13 selective catalytic reduction catalysts, J. Catal. 378 (2019) 363–375.

[50] D. Wang, F. Gao, C.H.F. Peden, J.H. Li, K. Kamasamudram, W.S. Epling, Selective catalytic reduction of NOx with NH3 over a Cu-SSZ-13 catalyst prepared by a solid-state ion-exchange method, Chemcatchem 6 (2014) 1579–1583.

[51] J. Hafner, Ab-initio simulations of materials using VASP, Density-Funct. Theory Beyond 29 (2008) 2044–2078.

[52] R. Zhang, J.-S. McEwen, M. Kollár, F. Gao, Y. Wang, J. Szanyi, C.H.F. Peden, N. O. Chemisorption, on Cu/SSZ-13: a comparative study from infrared spectroscopy and DFT calculations, Acs Catal. 4 (2014) 4093–4105.

[53] C. Paolucci, A.A. Verma, S.A. Bates, V.F. Kispersky, J.T. Miller, R. Gounder, W. N. Delgass, F.H. Ribeiro, W.F. Schneider, Isolation of the copper redox steps in the standard selective catalytic reduction on Cu-SSZ-13, Angew. Chem. Int. Ed. 53 (2014) 11828–11833.

[54] J.S. McEwen, T. Anggara, W.F. Schneider, V.F. Kispersky, J.T. Miller, W.N. Delgass, F.H. Ribeiro, Integrated operando X-ray absorption and DFT characterization of Cu–SSZ-13 exchange sites during the selective catalytic reduction of NOx with NH3, Catal. Today 184 (2012) 129–144.

[55] M. Yu, D.R. Trinkle, Accurate and efficient algorithm for Bader charge integration, The, J. Chem. Phys. 134 (2011) 064111.

[56] S. Posysaev, O. Miroshnichenko, M. Alatalo, D. Le, T.S. Rahman, Oxidation states of binary oxides from data analytics of the electronic structure, Comput. Mater. Sci. 161 (2019) 403–414.

[57] X. Wang, Y. Xu, M. Qin, Z. Zhao, X. Fan, Q. Li, Insight into the effects of Cu2+ ions and CuO species in Cu-SSZ-13 catalysts for selective catalytic reduction of NO by NH3, J. Colloid Interface Sci. 622 (2022) 1–10.

[58] B. Kerkeni, D. Berthout, D. Berthomieu, D.E. Doronkin, M. Casapu, J.D. Grunwaldt, C. Chizallet, Copper coordination to water and ammonia in cuii-exchanged SSZ-13: atomistic insights from DFT calculations and in situ XAS experiments, J. Phys. Chem. C 122 (2018) 16741–16755.

[59] C.W. Andersen, M. Bremholm, P.N.R. Vennestrøm, A.B. Blichfeld, L.F. Lundegaard, B.B. Iversen, Location of Cu2+ in CHA zeolite investigated by X-ray diffraction using the Rietveld/maximum entropy method, IUCrJ 1 (2014) 382–386.

[60] E. Borfecchia, P. Beato, S. Svelle, U. Olsbye, C. Lamberti, S. Bordiga, Cu-CHA - a model system for applied selective redox catalysis, Chem. Soc. Rev. 47 (2018) 8097–8133.

[61] J.H. Kwak, H.Y. Zhu, J.H. Lee, C.H.F. Peden, J. Szanyi, Two different cationic positions in Cu-SSZ-13? Chem. Commun. 48 (2012) 4758–4760.

[62] Y.J. Kim, J.K. Lee, K.M. Min, S.B. Hong, I.S. Nam, B.K. Cho, Hydrothermal stability of CuSSZ13 for reducing NOx by NH3, J. Catal. 311 (2014) 447–457.

[63] F. Gao, Y.L. Wang, N.M. Washton, M. Kollar, J. Szanyi, C.H.F. Peden, Effects of alkali and alkaline earth cocations on the activity and hydrothermal stability of Cu/SSZ-13 NH3-SCR catalysts, ACS Catal. 5 (2015) 6780–6791.

[64] Z.C. Zhao, R. Yu, R.R. Zhao, C. Shi, H. Gies, F.S. Xiao, D. De Vos, T. Yokoi, X. H. Bao, U. Kolb, M. Feyen, R. McGuire, S. Maurer, A. Moini, U. Muller, W.P. Zhang, Cu-exchanged Al-rich SSZ-13 zeolite from organotemplate-free synthesis as NH3-SCR catalyst: effects of Na+ ions on the activity and hydrothermal stability, Appl. Catal. B-Environ. 217 (2017) 421–428.

[65] R. Villamaina, S.J. Liu, I. Nova, E. Tronconi, M.P. Ruggeri, J. Collier, A. York, D. Thompsett, Speciation of Cu cations in Cu-CHA catalysts for NH3-SCR: effects of SiO2/AlO3 ratio and Cu-loading investigated by transient response methods, ACS Catal. 9 (2019) 8916–8927.

[66] J.P. Du, Y.L. Shan, Y. Sun, M. Gao, Z.Q. Liu, X.Y. Shi, Y.B. Yu, H. He, Unexpected increase in low-temperature NH3-SCR catalytic activity over Cu-SSZ-39 after hydrothermal aging, Appl. Catal. B-Environ. 294 (2021).

[67] Y.R. Cui, Y.L. Wang, E.D. Walter, J. Szanyi, Y. Wang, F. Gao, Influences of Na+ co-cation on the structure and performance of Cu/SSZ-13 selective catalytic reduction catalysts, Catal. Today 339 (2020) 233–240.

[68] J.E. Schmidt, R. Oord, W. Guo, J.D. Poplawsky, B.M. Weckhuysen, Nanoscale tomography reveals the deactivation of automotive copper-exchanged zeolite catalysts, Nat. Commun. 8 (2017).

[69] Y.Q. Wu, T. Andana, Y.L. Wang, Y. Chen, E.D. Walter, M.H. Engelhard, K.G. Rappe, Y. Wang, F. Gao, U. Menon, R. Daya, D. Trandal, H.M. An, Y.H. Zha, K. Kamasamudram, A comparative study between real-world and laboratory accelerated aging of Cu/SSZ-13 SCR catalysts, Appl. Catal. B-Environ. 318 (2022).

[70] P.N.R. Vennestrom, T.V.W. Janssens, A. Kustov, M. Grill, A. Puig-Molina, L. F. Lundegaard, R.R. Tiruvalam, P. Concepcion, A. Corma, Influence of lattice stability on hydrothermal deactivation of Cu-ZSM-5 and Cu-IM-5 zeolites for selective catalytic reduction of NOx by NH3, J. Catal. 309 (2014) 477–490.

[71] J. Song, Y.L. Wang, E.D. Walter, N.M. Washton, D.H. Mei, L. Kovarik, M. H. Engelhard, S. Prodinger, Y. Wang, C.H.F. Peden, F. Gao, Toward rational design of Cu/SSZ-13 selective catalytic reduction catalysts: implications from atomic-level understanding of hydrothermal stability, ACS Catal. 7 (2017) 8214–8227.

[72] Y.N. Zhang, Y. Peng, J.H. Li, K. Groden, J.S. Mcewen, E.D. Walter, Y. Chen, Y. Wang, F. Gao, Probing active-site relocation in Cu/SSZ-13 SCR catalysts during hydrothermal aging by in situ EPR spectroscopy, kinetics studies, and DFT calculations, ACS Catal. 10 (2020) 9410–9419.

[73] F. Gao, C.H.F. Peden, Recent progress in atomic-level understanding of Cu/SSZ-13 selective catalytic reduction catalysts, Catalysts 8 (2018) 140.

[74] M. Colombo, I. Nova, E. Tronconi, A comparative study of the NH(3)-SCR reactions over a Cu-zeolite and a Fe-zeolite catalyst, Catal. Today 151 (2010) 223–230.

[75] B. Ipek, M.J. Wulfers, H. Kim, F. Goltl, I. Hermans, J.P. Smith, K.S. Booksh, C. M. Brown, R.F. Lobo, Formation of [Cu2O2](2+) and [Cu2O](2+) toward C-H bond activation in Cu-SSZ-13 and Cu-SSZ-39, Acs Catal. 7 (2017) 4291–4303.

[76] C. Negri, M. Signorile, N.G. Porcaro, E. Borfecchia, G. Berlier, T.V.W. Janssens, S. Bordiga, Dynamic Cu-II/Cu-I speciation in Cu-CHA catalysts by in situ diffuse reflectance UV–vis-NIR spectroscopy, Appl. Catal. A-Gen. 578 (2019) 1–9.

[77] H. Li, C. Paolucci, I. Khurana, L. Wilcox, F. Goltl, J.D. Albarracin-Caballero, A. J. Shih, F.H. Ribeiro, R. Gounder, W.F. Schneider, Consequences of exchange-site heterogeneity and dynamics on the UV–visible spectrum of Cu-exchanged SSZ-13, Chem. Sci. 10 (2019) 2373–2384.

[78] Y.N. Zhang, J. Zhang, H.L. Wang, W.N. Yang, C.Z. Wang, Y. Peng, J.J. Chen, J. H. Li, F. Gao, Selective catalytic reduction of NOx with NH3 over Cu/SSZ-13: elucidating dynamics of Cu active sites with in situ UV-vis spectroscopy and DFT calculations, J. Phys. Chem. C 126 (2022) 8720–8733.

[79] E. Borfecchia, K.A. Lomachenko, F. Giordanino, H. Falsig, P. Beato, A.V. Soldatov, S. Bordiga, C. Lamberti, Revisiting the nature of Cu sites in the activated Cu-SSZ-13 catalyst for SCR reaction, Chem. Sci. 6 (2015) 548–563.

[80] H.Y. Chen, Z.H. Wei, M. Kollar, F. Gao, Y.L. Wang, J. Szanyi, C.H.F. Peden, A comparative study of N2O formation during the selective catalytic reduction of NOx with NH3 on zeolite supported Cu catalysts, J. Catal. 329 (2015) 490–498.

[81] D.W. Yao, B.A. Liu, F. Wu, Y.X. Li, X.H. Hu, W.Y. Jin, X.L. Wang, N2O formation mechanism during low-temperature NH3-SCR over Cu/SSZ-13 catalysts with different Cu loadings, Ind. Eng. Chem. Res 60 (2021) 10083–10093.

[82] P. Forzatti, I. Nova, E. Tronconi, Enhanced NH3 selective catalytic reduction for NOx abatement, Angew. Chem. Int Ed. 48 (2009) 8366–8368.

[83] D. Zhang, R.T. Yang, N2O formation pathways over zeolite-supported Cu and Fe catalysts in NH3-SCR, Energy Fuel 32 (2018) 2170–2182.

[84] M. Colombo, I. Nova, E. Tronconi, Detailed kinetic modeling of the NH3-NO/NO2 SCR reactions over a commercial Cu-zeolite catalyst for Diesel exhausts after treatment, Catal. Today 197 (2012) 243–255.

[85] M. Bendrich, A. Scheuer, R.E. Hayes, M. Votsmeier, Unified mechanistic model for Standard SCR, Fast SCR, and NO2 SCR over a copper chabazite catalyst, Appl. Catal. B-Environ. 222 (2018) 76–87.

[86] Y.X. Feng, T.V.W. Janssens, P.N.R. Vennestrom, J. Jansson, M. Skoglundh, H. Gronbeck, The role for N2O formation during NH3-SCR over Cu-CHA, J. Phys. Chem. C 125 (2021) 4595–4601.

[87] A.J. Shih, J.M. Gonzalez, I. Khurana, L.P. Ramirez, L.A. Pena, A. Kumar, A.L. Villa, Influence of ZCuOH, Z(2)Cu, and extraframework CuxOy species in Cu-SSZ-13 on N2O formation during the selective catalytic reduction of NOx with NH3, ACS Catal. 11 (2021) 10362–10376.

[88] Y.Z. Xi, N.A. Ottinger, C.J. Keturakis, Z.G. Liu, Dynamics of low temperature N2O formation under SCR reaction conditions over a Cu-SSZ-13 catalyst, Appl. Catal. B-Environ. 294 (2021).

[89] L. Negahdar, N.E. Omori, M.G. Quesne, M.D. Frogley, F. Cacho-Nerin, W. Jones, S. W.T. Price, C.R.A. Catlow, A.M. Beale, Elucidating the significance of copper and nitrate speciation in Cu-SSZ-13 for N2O formation during NH3-SCR, ACS Catal. 11 (2021) 13091–13101.

[90] U. Deka, I. Lezcano-Gonzalez, S.J. Warrender, A.L. Picone, P.A. Wright, B. M. Weckhuysen, A.M. Beale, Changing active sites in Cu-CHA catalysts: deNO(x) selectivity as a function of the preparation method, Microporous Mesoporous Mater. 166 (2013) 144–152.

[91] Y. Ma, X.D. Wu, J.C. Ding, L.P. Liu, B.F. Jin, E.D. Walter, R. Ran, Z.C. Si, F. Gao, D. Weng, Quasi-operando quantification of Cu(ii) ions in Cu-SSZ-13 catalyst by an NH3 temperature-programmed reduction method, Chem. Commun. 57 (2021) 1891–1894.

[92] M.P. Ruggeri, S. Tommaso, C. Massimo, I. Nova, E. Tronconi, Identification of nitrites/HONO as primary products of NO oxidation over Fe-ZSM-5 and their role in the Standard SCR mechanism: a chemical trapping study, J. Catal. 311 (2014) 266–270.

[93] C. Paolucci, A.A. Verma, S.A. Bates, V.F. Kispersky, J.T. Miller, R. Gounder, W. N. Delgass, F.H. Ribeiro, W.F. Schneider, Isolation of the copper redox steps in the standard selective catalytic reduction on Cu-SSZ-13, Angew. Chem. Int. Ed. 53 (2014) 11828–11833.